The Abdus Salam International Centre for Theoretical Physics
50th Anniversary 1964-2014

2585-3

Joint ICTP-TWAS School on Coherent State Transforms, Time-Frequency and Time-Scale Analysis, Applications

2 - 20 June 2014

Wavelet-based multifractal analysis of dynamic IR thermograms and X-ray mammograms to assist in early breast cancer diagnosis

A. Arneodo
ENS, Lyon
France

Wavelet-based multifractal analysis of dynamic IR thermograms and X-ray mammograms to assit in early breast cancer diagnosis

Alain Arneodo

Laboratoire de Physique, Ecole Normale Supérieure de Lyon

Alain.Arneodo@ens-lyon.fr

Mammograms

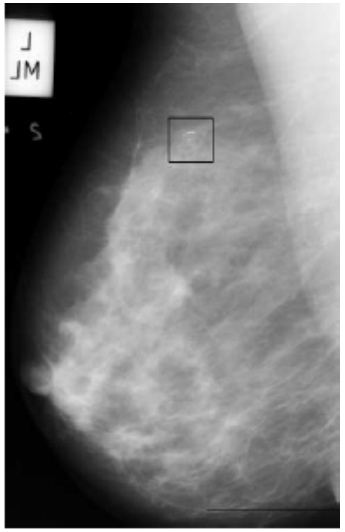

Calcifications

Thermograms

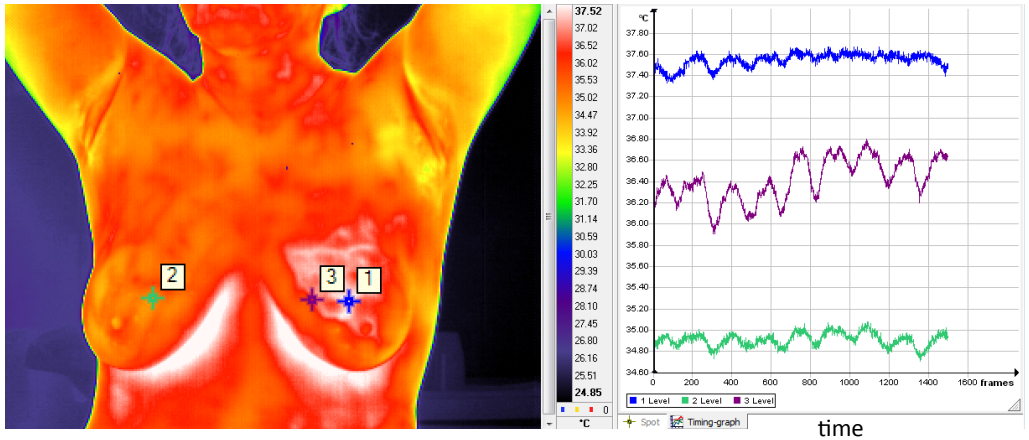

time

Wavelet-based multifractal analysis of rough surfaces
The 2D Wavelet Transform Modulus Maxima (WTMM) method

Alain Arneodo

Nicolas Decoster — Centre de Recherche Paul Pascal, Bordeaux

Stéphane G. Roux

Pierre Kesterner — Ecole Normale Supérieure de Lyon

Sand-blasted brass surface

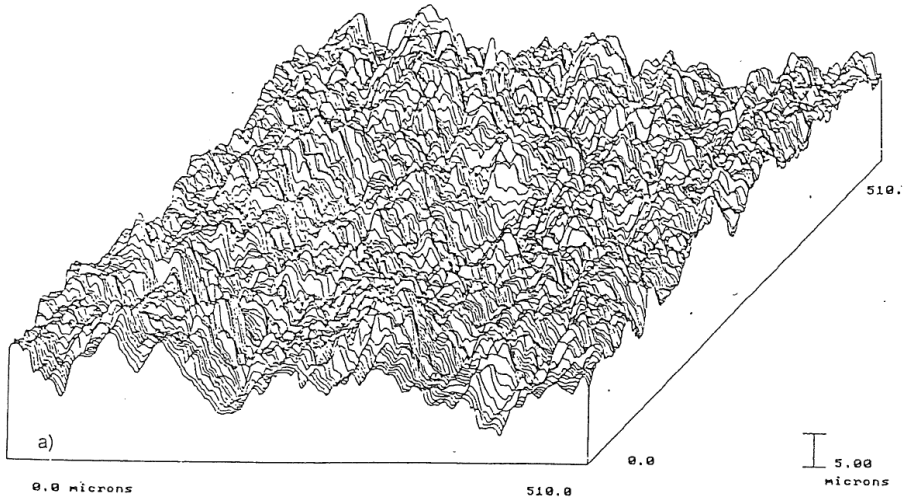

Vapor-deposited silver films

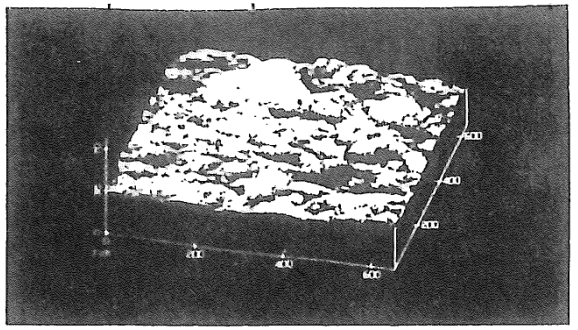

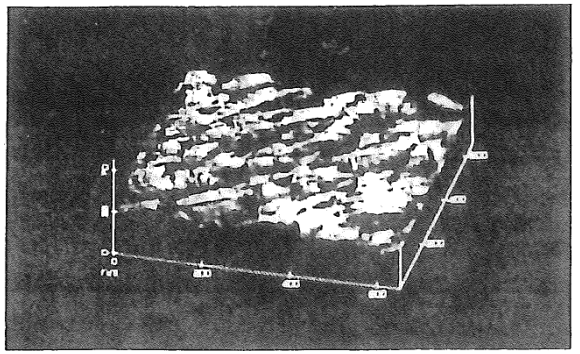

Fatigued Polycrystalline Copper

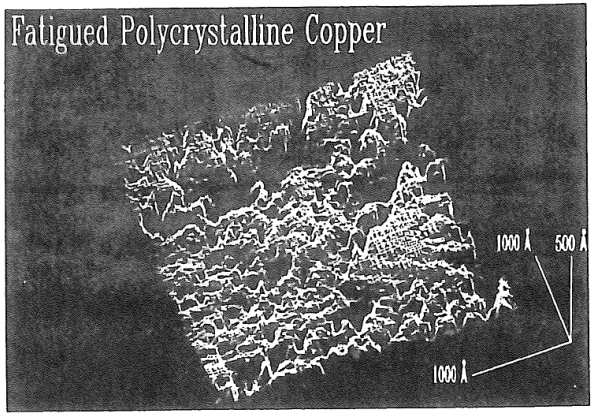

Mountain landscape

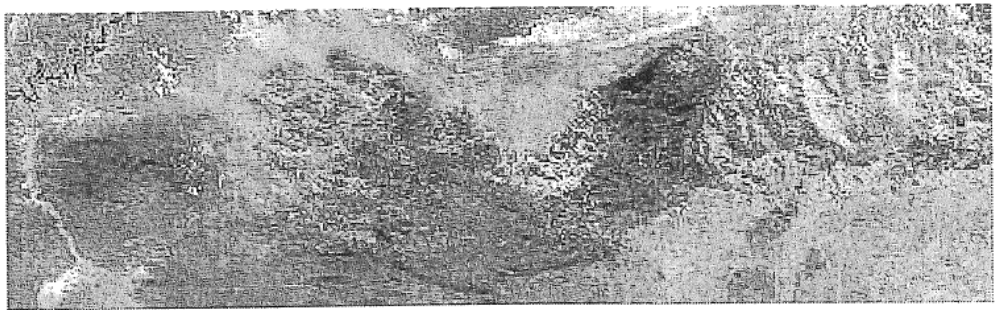

Clouds

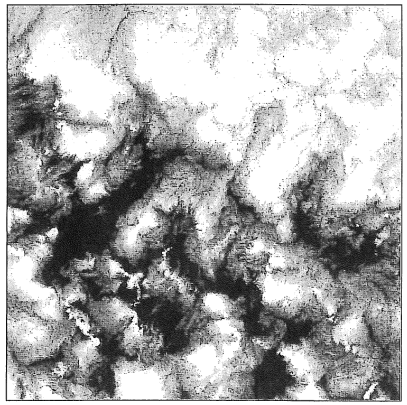

Fully developed turbulence

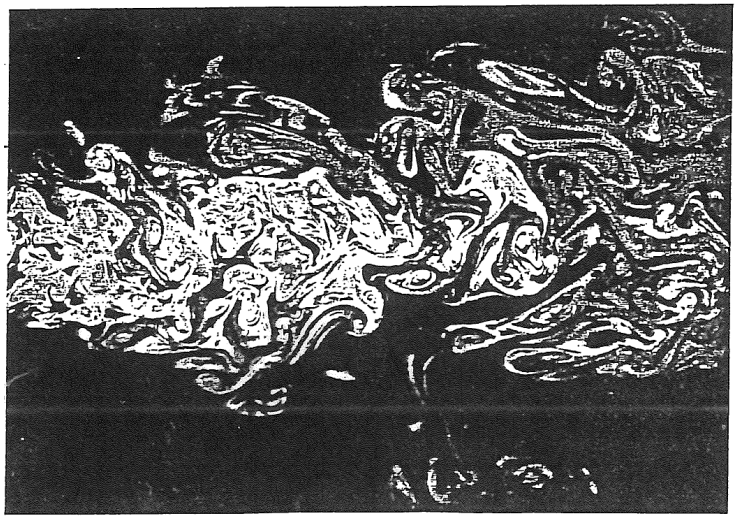

Mammograms

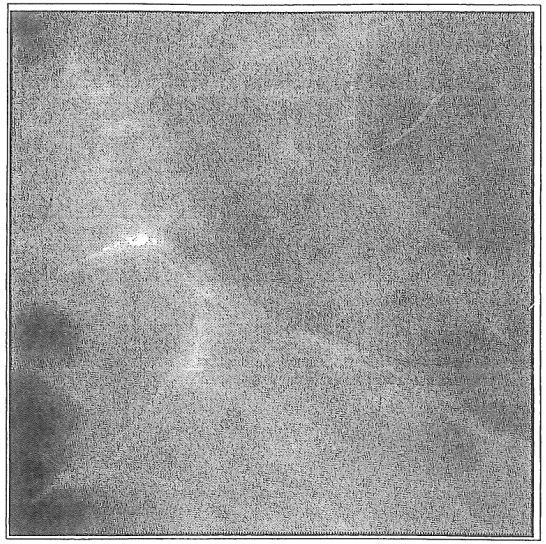

Fractal Objects : self-similarity

- exact self-similarity :

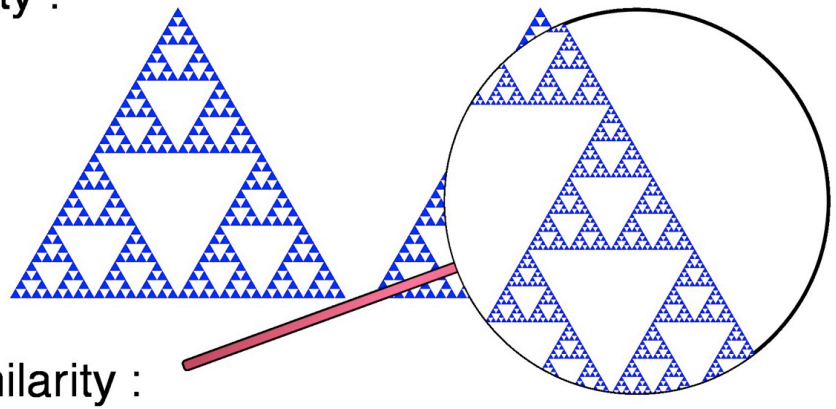

- statistical self-similarity :

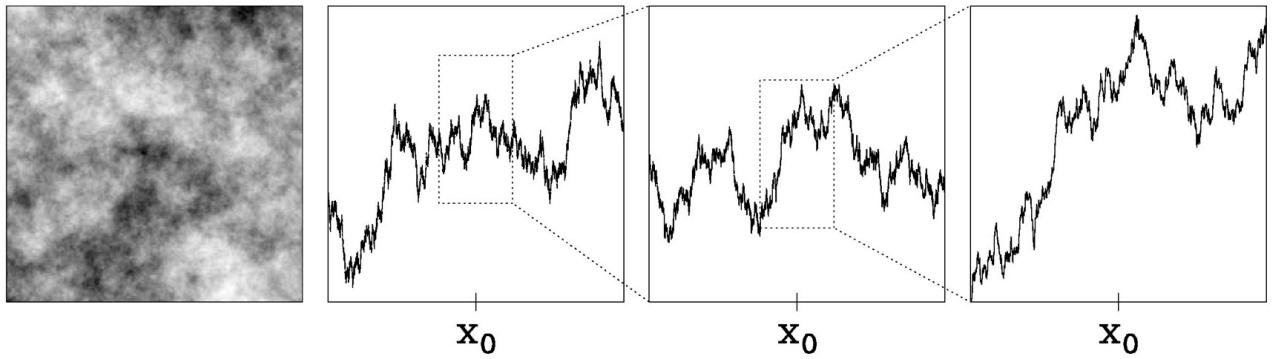

$$f(x_0 + \lambda u) - f(x_0) \sim \lambda^{h(x_0)} (f(x_0 + u) - f(x_0))$$

2D WTMM Methodology : PhD work of N. Decoster

2D data : I

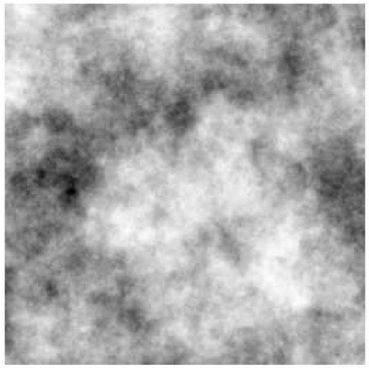

Smoothing scale a

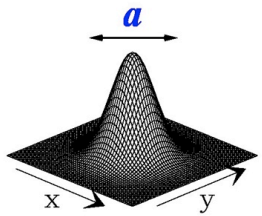

Gradient ∇

$$\left[\frac{\partial}{\partial x}, \frac{\partial}{\partial y}\right]$$

Wavelet Transform

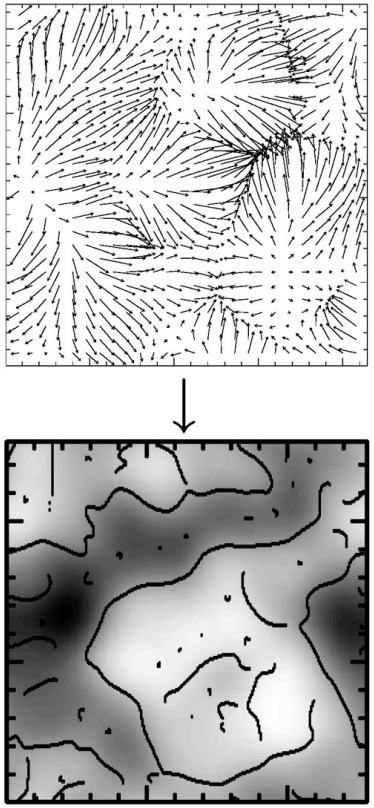

$$\mathbf{T}_\psi(\mathbf{r}, a) = \begin{pmatrix} I * \frac{\partial \phi_a}{\partial x}(\mathbf{r}) \\ I * \frac{\partial \phi_a}{\partial y}(\mathbf{r}) \end{pmatrix}$$

$$\mathbf{T}_\psi(\mathbf{r}, a) = \nabla(I * \phi_a)(\mathbf{r}) = (\mathcal{M}_\psi(\mathbf{r}, a), \mathcal{A}_\psi(\mathbf{r}, a))$$

$$\psi_1(x,y) = \frac{\partial \phi(x,y)}{\partial x}$$

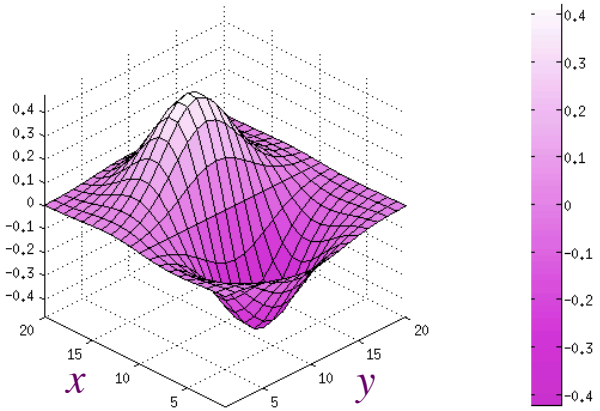

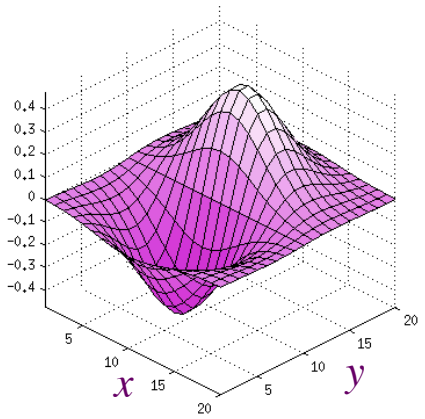

$$\psi_2(x,y) = \frac{\partial \phi(x,y)}{\partial y}$$

WTMM Methodology : Skeleton

WTMM Chains

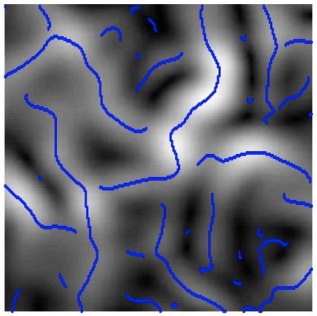

WTMMM

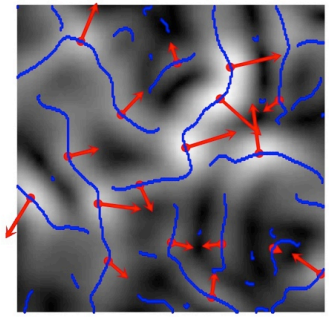

WTMM Chains at 3 different scales

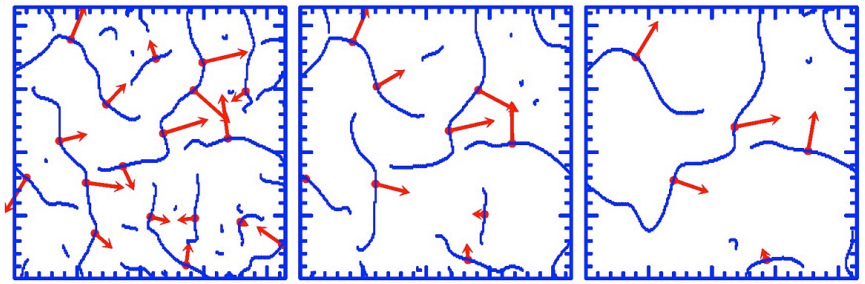

WTMMM Chaining : WT skeleton

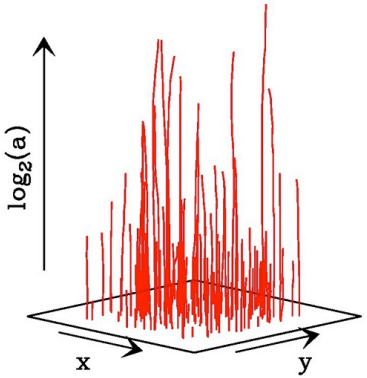

- **Monofractal Image**

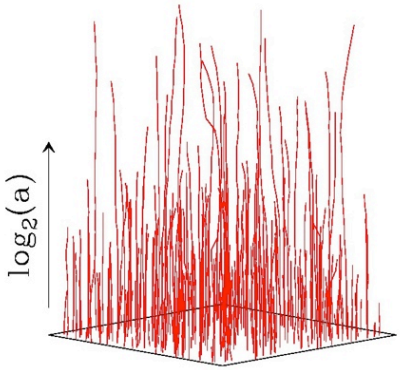

$\mathcal{M} \sim a^{h}$,
single h

- **Multifractal Image**

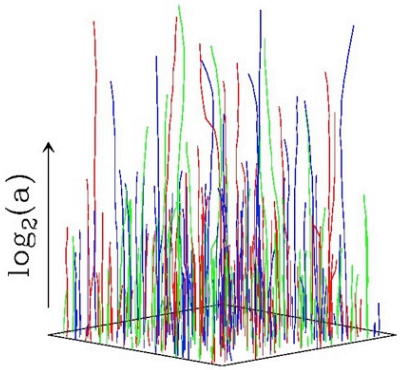

$\mathcal{M} \sim a^{h}, a^{h}, a^{h},$
$h \in [h_{\min}, h_{\max}]$

WTMM Method : multifractal formalism

Singularity spectrum :

$$D(h) = d_H\{\mathrm{r} \in R^d, h(\mathrm{r}) = h\}$$

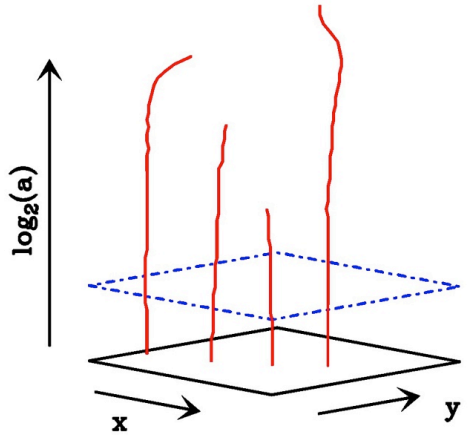

Legendre transform :

$$D(h) = \min_q \left(qh - \tau(q) \right)$$

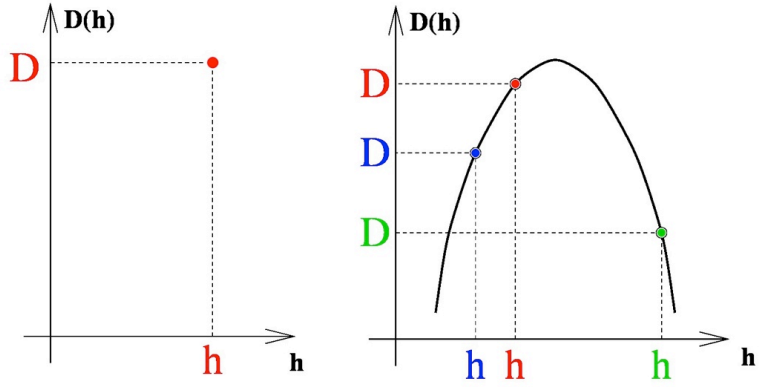

Analogy statistical physics : compute partition functions

$$\mathcal{Z}(q,a) = \sum_{\mathcal{L}(a)} \left(\mathcal{M}_\psi(\mathrm{r},a) \right)^q \sim a^{\tau(q)}$$

$$\mathcal{H}(q,a) = \sum_{\mathcal{L}(a)} \ln \left| \mathcal{M}_\psi(\mathrm{r},a) \right| \mathcal{W}_\psi(\mathrm{r},a) \sim a^{h(q)}$$

$$\mathcal{D}(q,a) = \sum_{\mathcal{L}(a)} \ln \left| \mathcal{W}_\psi(\mathrm{r},a) \right| \mathcal{W}_\psi(\mathrm{r},a) \sim a^{D(q)}$$

Application to synthetic monofractal surfaces

fractional Brownian surfaces : $B_H(\mathrm{r})$

- $H < 0.5$: anti-correlated increments
- $H = 0.5$: non-correlated increments
- $H > 0.5$: correlated increments

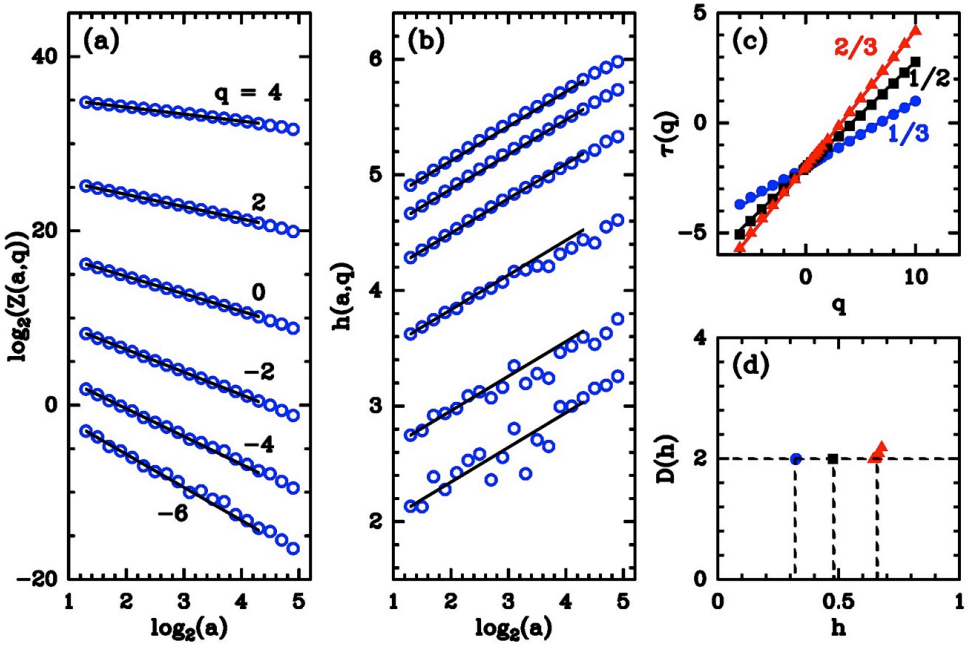

H=1/3

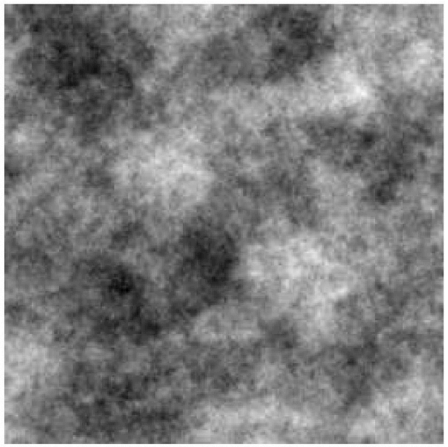

Theoretical Predictions :

- $\tau(q)$ is linear :
  $\tau(q) = qH - 2$
- multifractal spectrum is degenerated :
  $D(h = H) = 2$

Application to synthetic multifractal surfaces

Multifractal (Fractionally Integrated Singular Cascades) surfaces

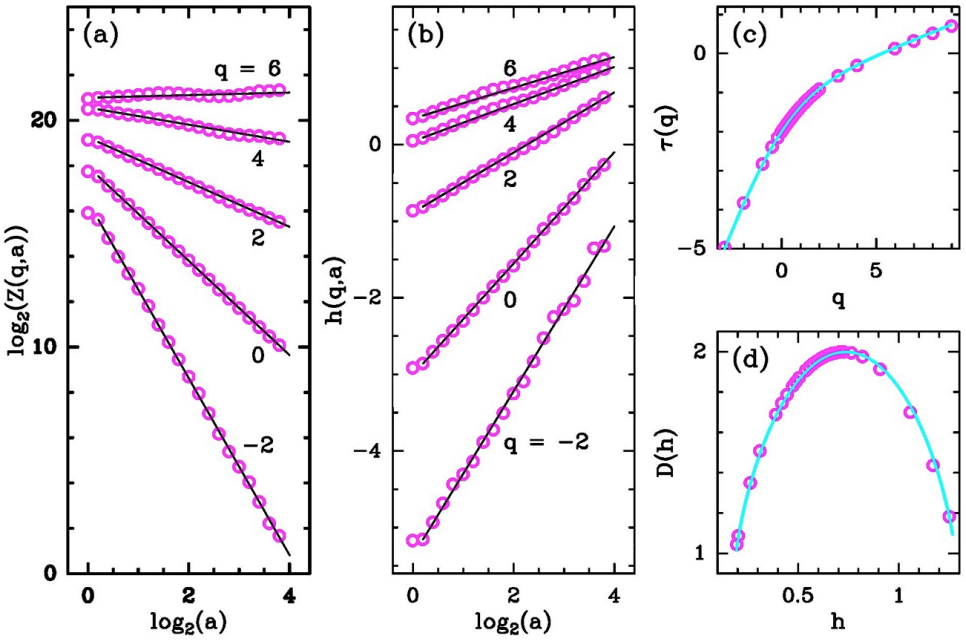

FISC

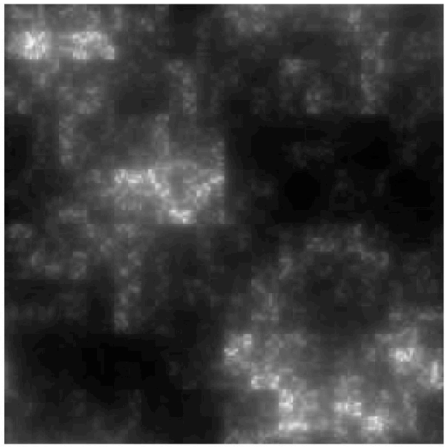

Theoretical predictions :

- $\tau(q)$ is non-linear

$$\tau(q) = -2 - q(1 - H^*) - \log_2(p_1{}^q + p_2{}^q)$$

- singularity spectrum is a non-degenerated convex curve

Application of the 2D WTMM method to mammography texture analysis and characterization of breast lesions

Alain Arneodo
Pierre Kesterner

Ecole Normale Supérieure de Lyon

André Khalil
Kendra Batchelder
Aaron Tanenbaum

ComputMaine Laboratory, University of Maine, Orono (USA)

Mammography and breast anatomy

Goals : using WTMM method to diagnosis help of breast cancer

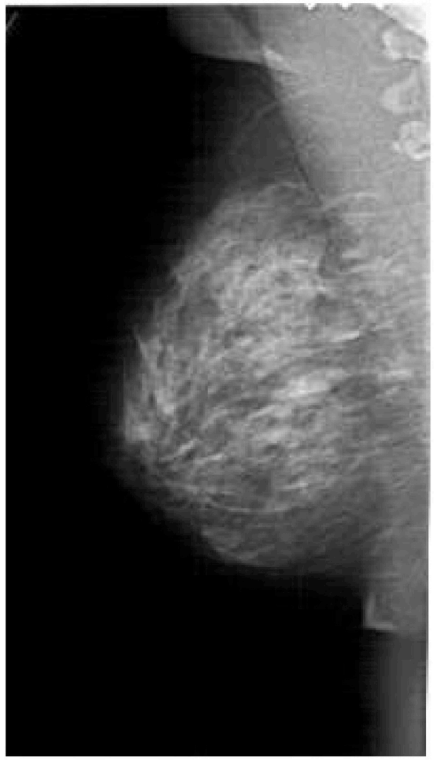

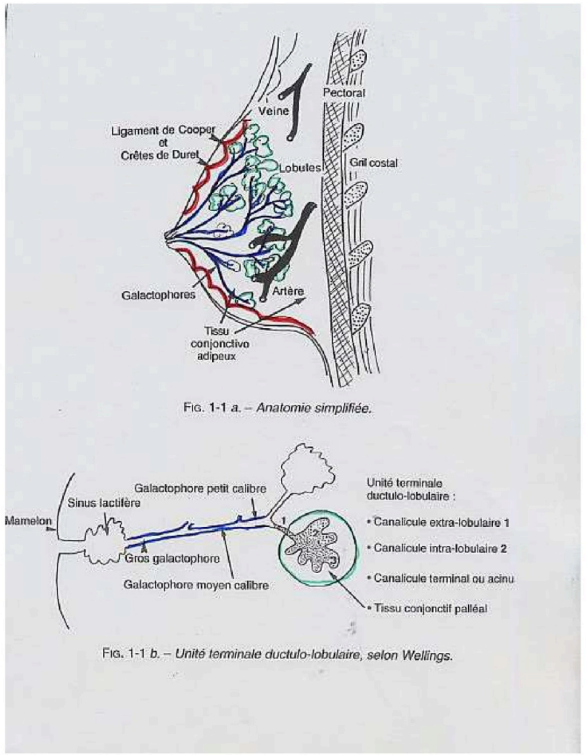

FIG. 1-1 *a.* – *Anatomie simplifiée.*

FIG. 1-1 *b.* – *Unité terminale ductulo-lobulaire, selon Wellings.*

Statistics

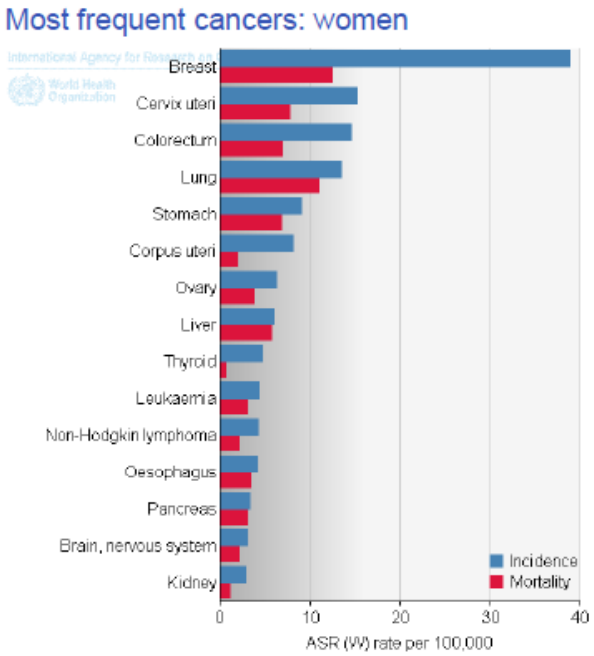
Most frequent cancers: women
Breast
Cervix uteri
Colorectum
Lung
Stomach
Corpus uteri
Ovary
Liver
Thyroid
Leukaemia
Non-Hodgkin lymphoma
Oesophagus
Pancreas
Brain, nervous system
Kidney
Incidence
Mortality
0
10
20
30
40
ASR (W) rate per 100,000

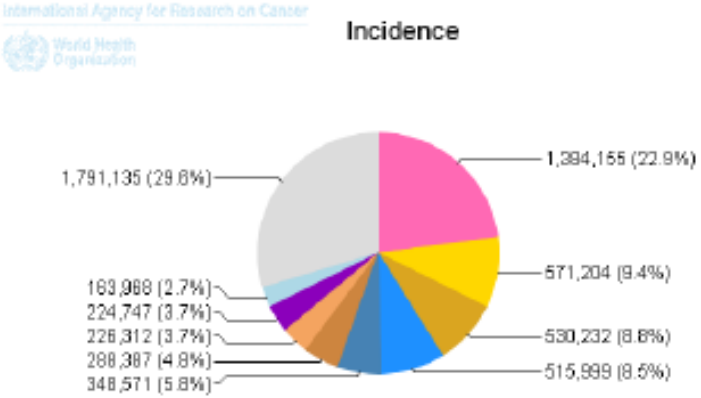
Incidence
1,791,135 (29.6%)
1,384,155 (22.9%)
571,204 (9.4%)
530,232 (8.8%)
515,999 (8.5%)
348,571 (5.8%)
288,387 (4.8%)
226,312 (3.7%)
224,747 (3.7%)
183,988 (2.7%)


Breast
Colorectum
Cervix uteri
Lung
Stomach
Corpus uteri
Liver
Ovary
Thyroid
Other and unspecified

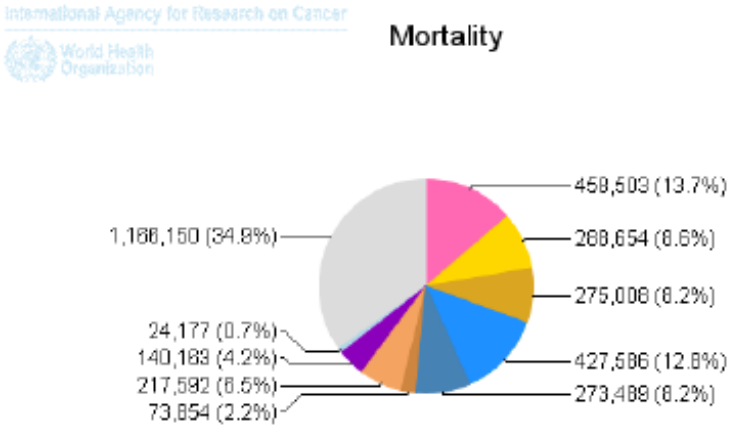
Mortality
1,166,150 (34.8%)
458,503 (13.7%)
288,654 (8.6%)
275,008 (8.2%)
427,586 (12.8%)
273,489 (8.2%)
73,854 (2.2%)
217,592 (6.5%)
140,183 (4.2%)
24,177 (0.7%)

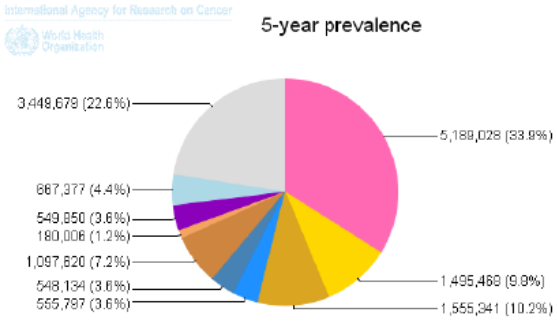
5-year prevalence
3,448,679 (22.6%)
5,189,028 (33.9%)
867,377 (4.4%)
549,850 (3.6%)
180,006 (1.2%)
1,097,820 (7.2%)
548,134 (3.6%)
555,797 (3.6%)
1,495,469 (9.8%)
1,555,341 (10.2%)

What is breast cancer ?

- malignant tumor of mammal gland
- incidence : 30000 new case each year in France
- prevention is very difficult (as opposed to lung cancer)
- hereditarity : 5 to 10 % only (BRCA1/2 genes)
- forecast depends on the tumoral volume at diagnosis

$\Rightarrow$ **SCREENING** using mammography

Screening Mammograms

- Currently the most effective way of detecting breast cancer
- Detects masses and microcalcifications (MC), which are small deposits of calcium in breast tissue and can be an early sign of breast cancer
- Radiologists associate certain patterns of MC deposits with benign and malignant tumors

Radiological anomalies

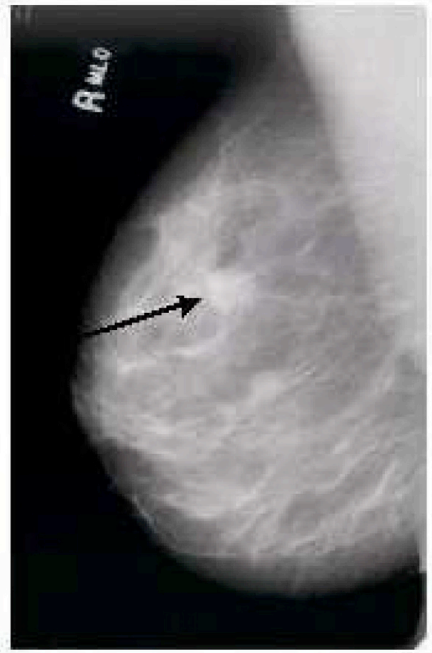

- Opacities

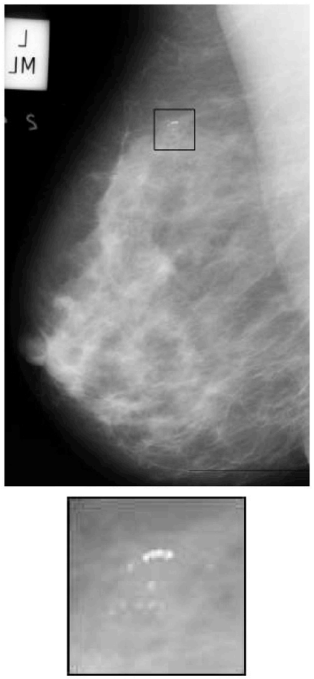

- Calcifications

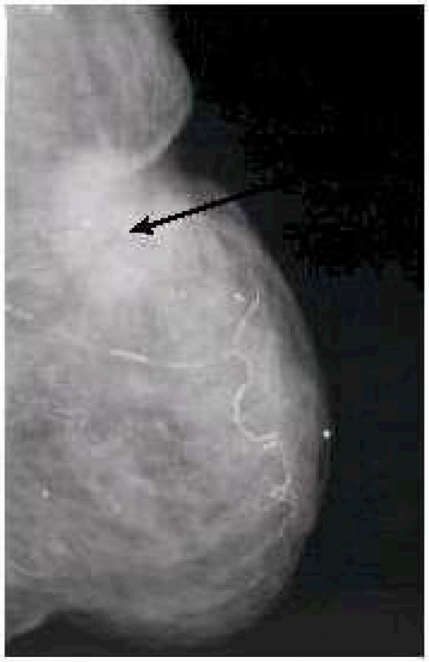

- Architectural distorcions

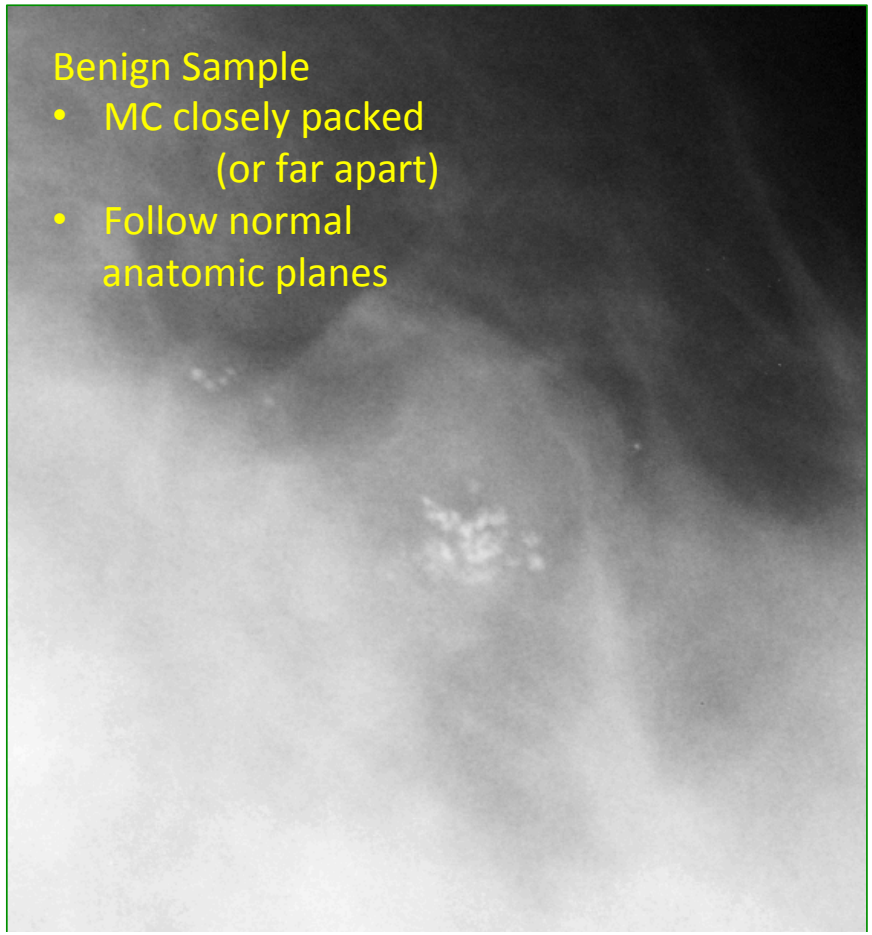
Benign Sample
• MC closely packed
(or far apart)
• Follow normal
anatomic planes

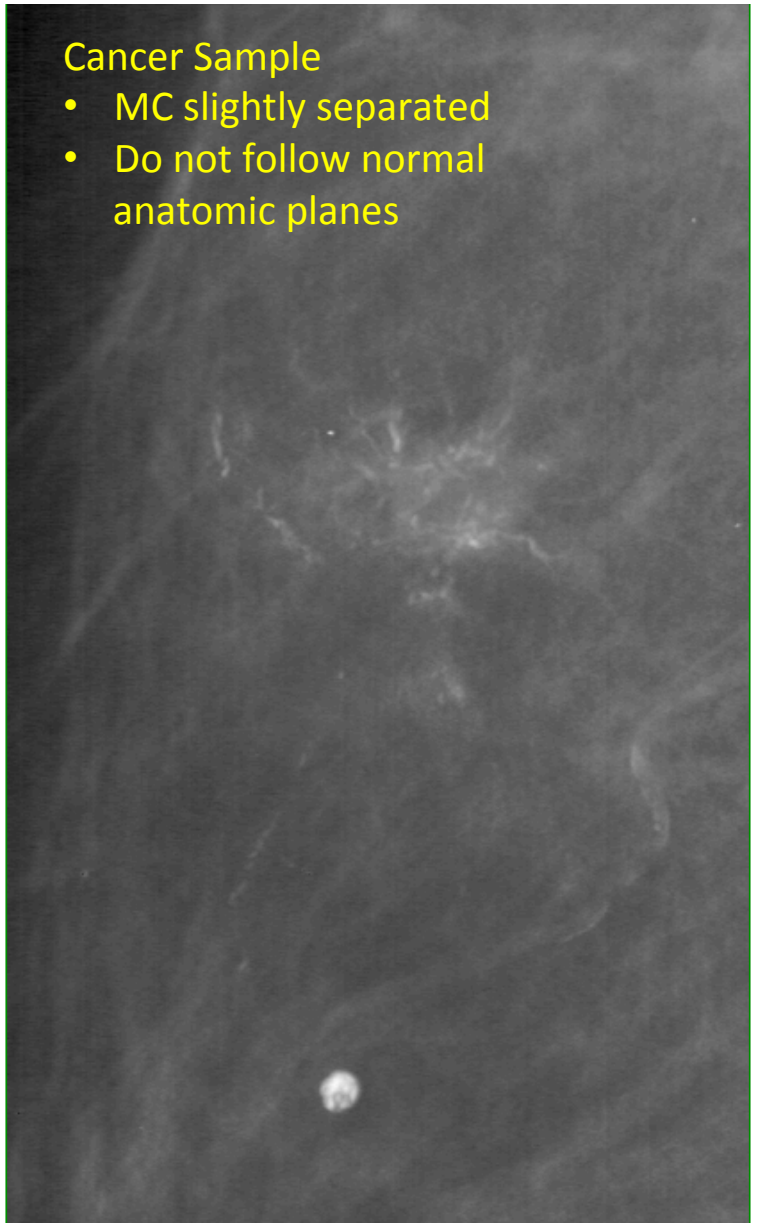
Cancer Sample
• MC slightly separated
• Do not follow normal
anatomic planes

Digitalized mammographies : texture analysis

- dense breasts : more difficult to diagnose
- only 2 classes of monofractal properties

Digital Database for Screening Mammography:

`http://marathon.csee.usf.edu/Mammography/Database.html`

Dense breast

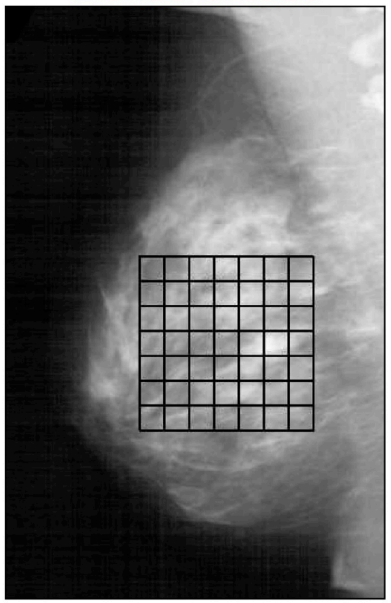

Fatty breast

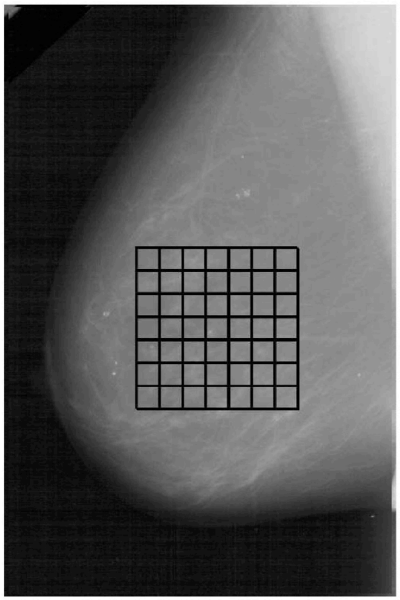

Application of 2D WTMM methodology in mammography

Tissue classification : dense

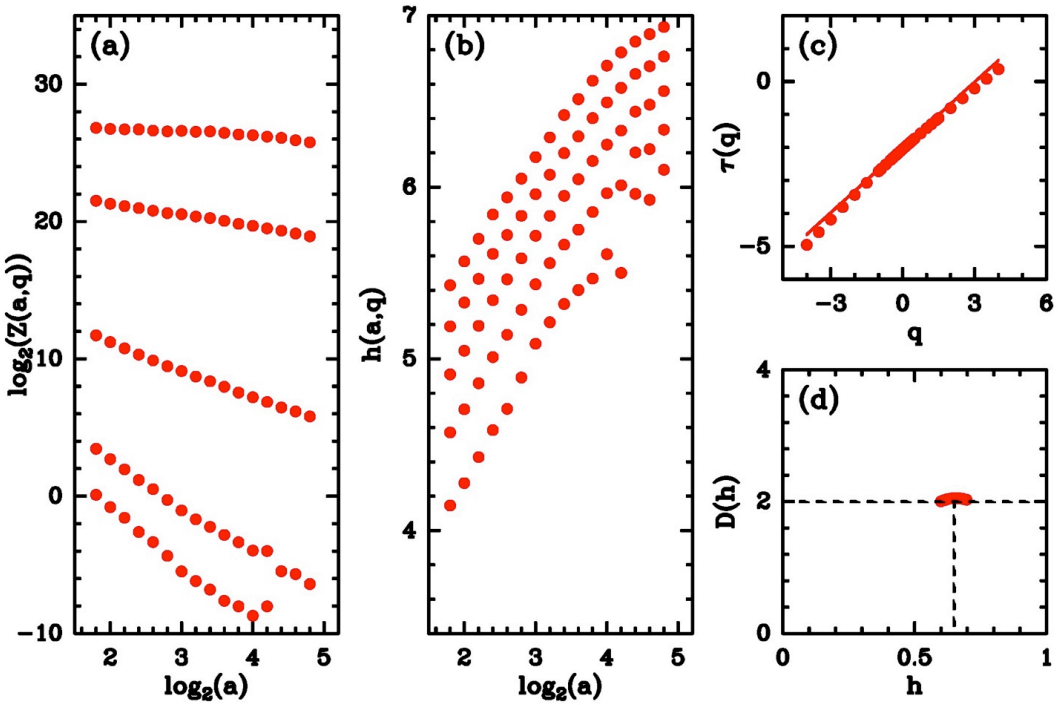

- **Dense breast :**
  monofractal, $H = 0.65$
  persitent correlations

Application of 2D WTMM methodology in mammography

Tissue classification : dense vs fatty

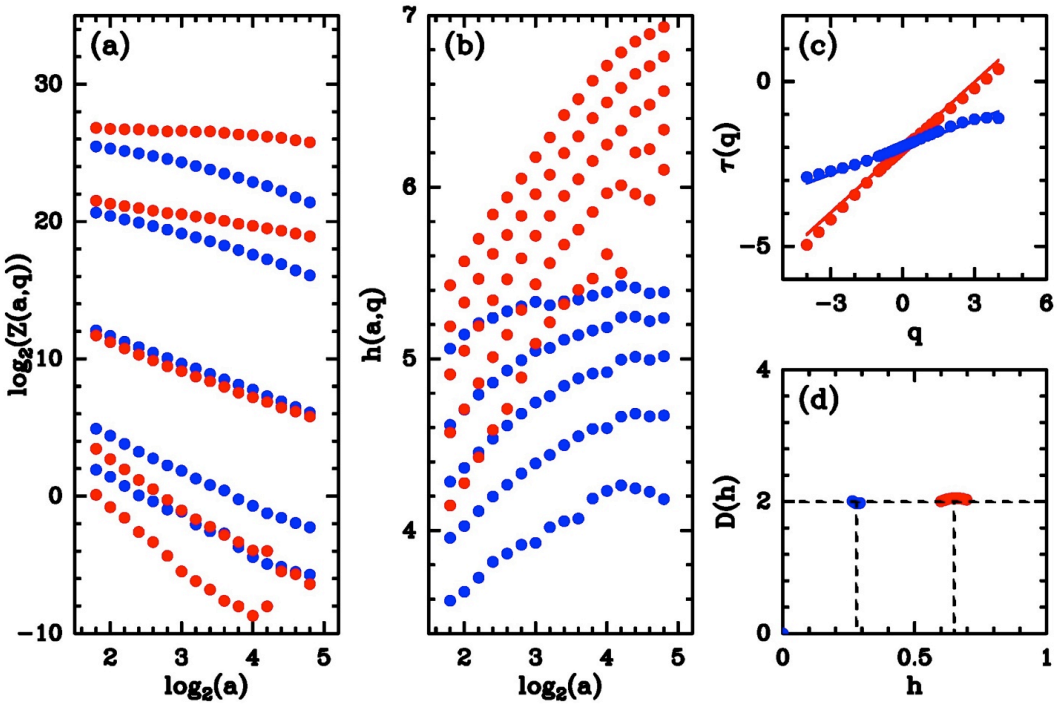

- Dense breast : monofractal, $H = 0.65$ persitent correlations
- Fatty breast : monofractal, $H = 0.30$ anti-persitent correlations

Application to digitalized mammographies

Colored Maps :
segmentation of dense $h > 0.52$ areas and fatty $h < 0.38$ areas

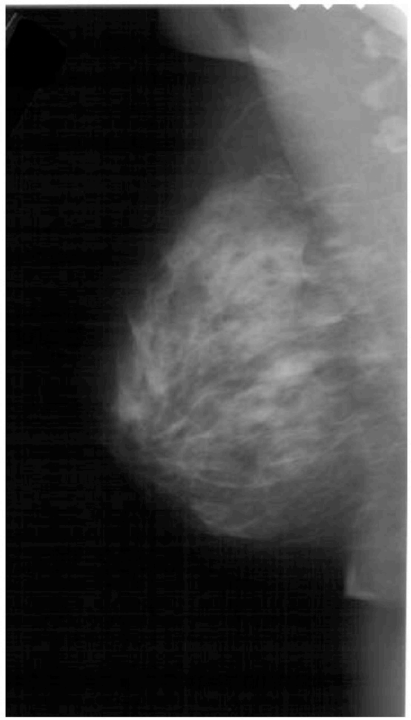

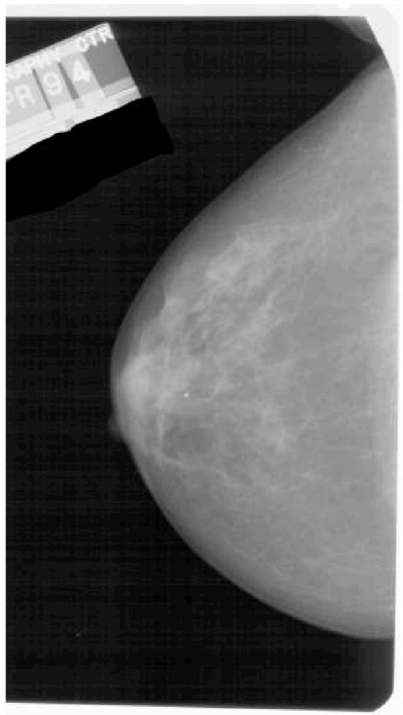

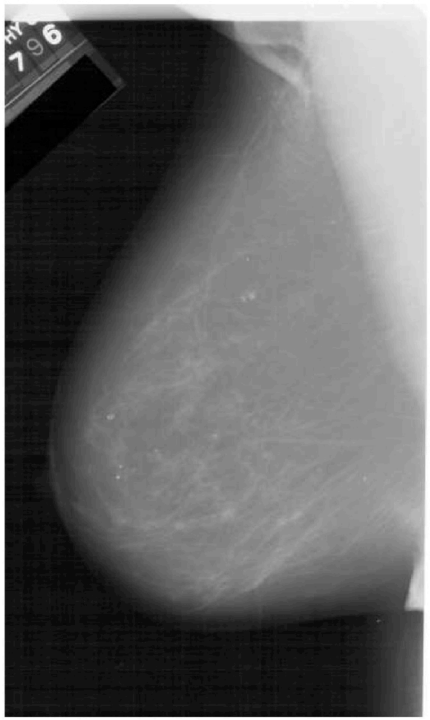

Application to digitalized mammographies

Colored Maps :
segmentation of dense $h > 0.52$ areas and fatty $h < 0.38$ areas

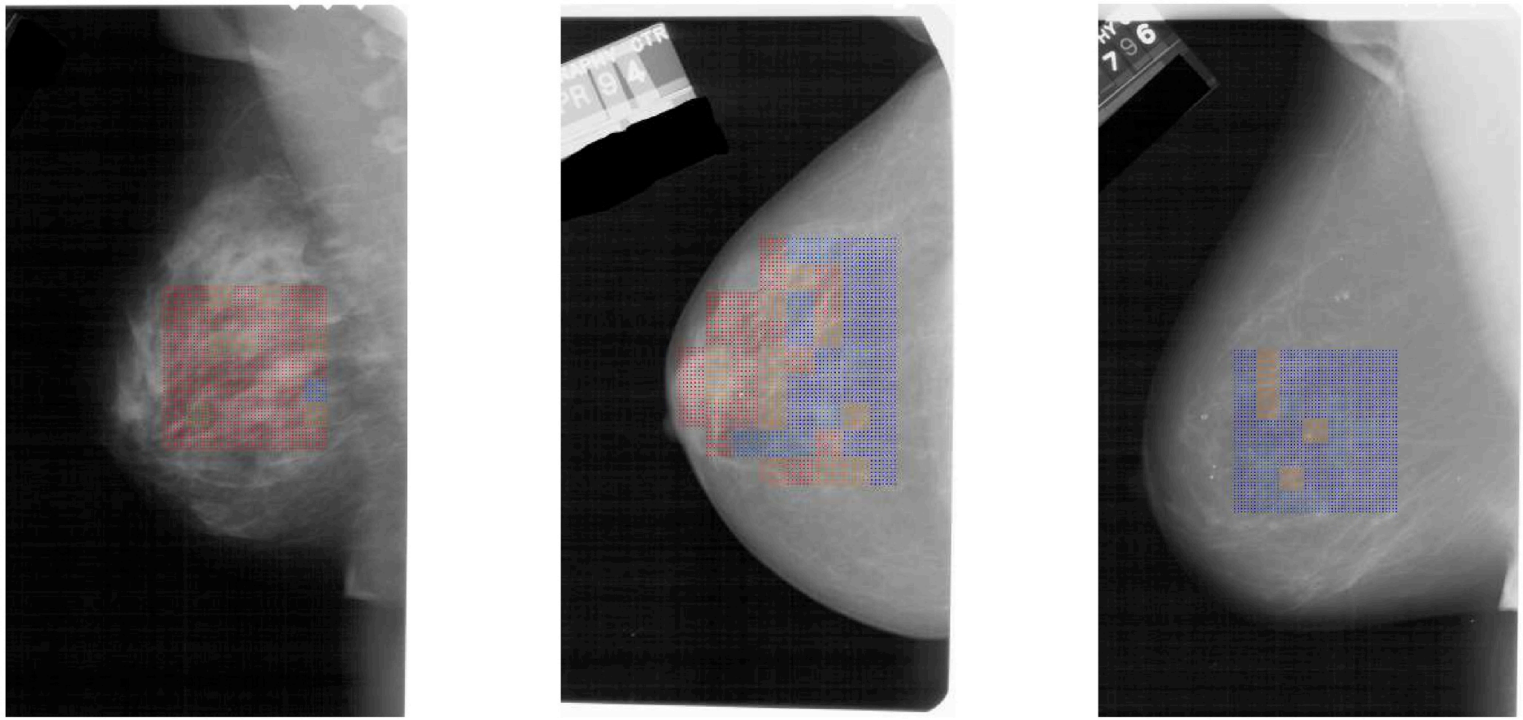

Microcalcifications detection

Segmentation of WT skeleton lines :
microcalcifications vs background texture

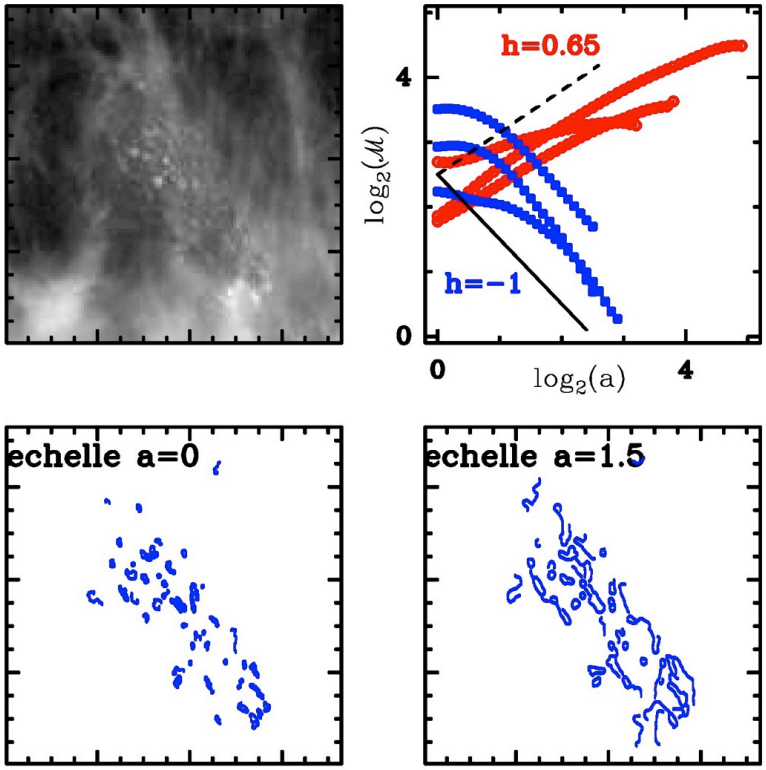

- Background lines
- Microcalcifications
  almost-punctual objects behave like 'Dirac' shapes ($h = -1$)

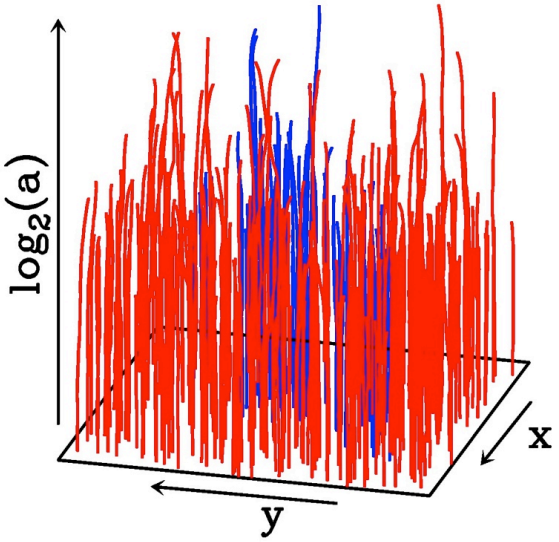

Cluster of microcalcifications

Study of microcalcification spatial distribution

Partition functions :

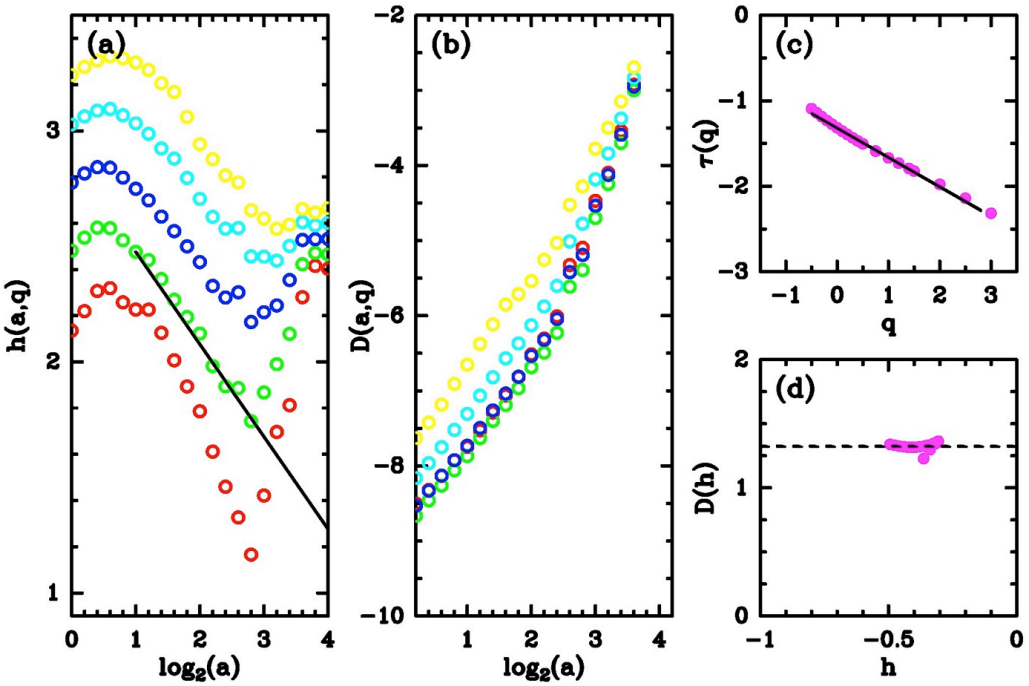

$$D_F = 1.3$$

observation :

fractal ramifi cation of cluster of microcalcifi cations ($1 < D_F < 2$) seems to be correlated to the pathology's malignancy

Two sided view analysis

- For each case:
  - 4 images
  - Fractal dimension (D) of the lesion for the MLO and CC view – Roughness (H) of the tissue that the lesion is embedded in for the MLO and CC view

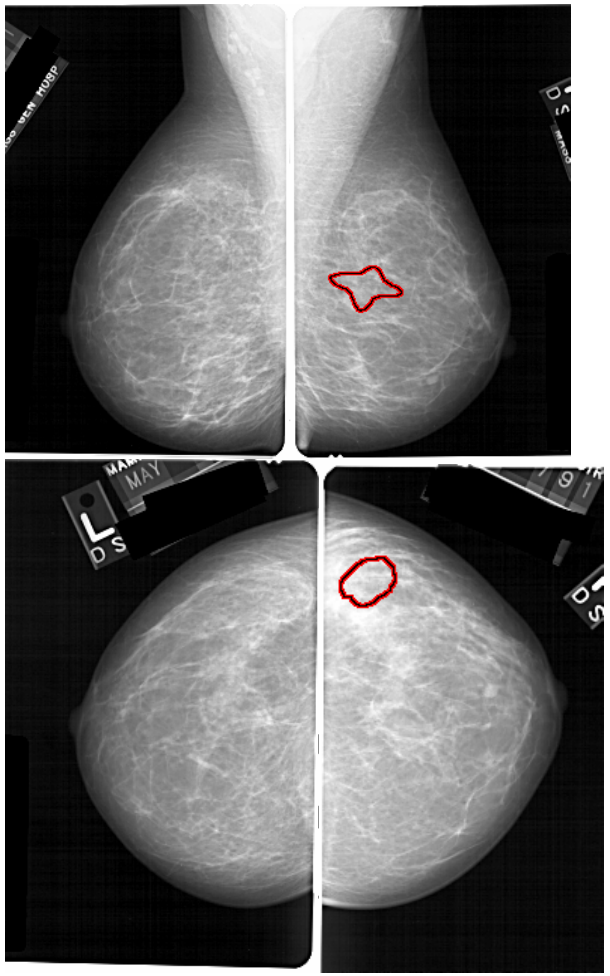

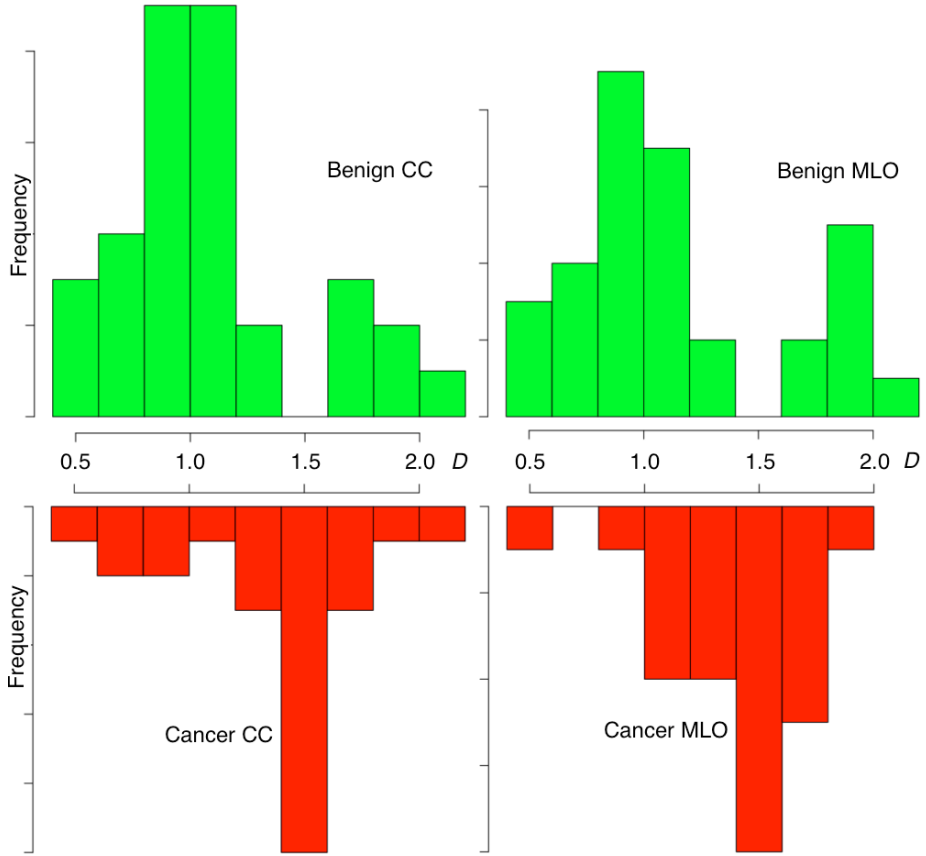
Frequency
Benign CC
Benign MLO
0.5
1.0
1.5
2.0
D
Frequency
Cancer CC
Cancer MLO

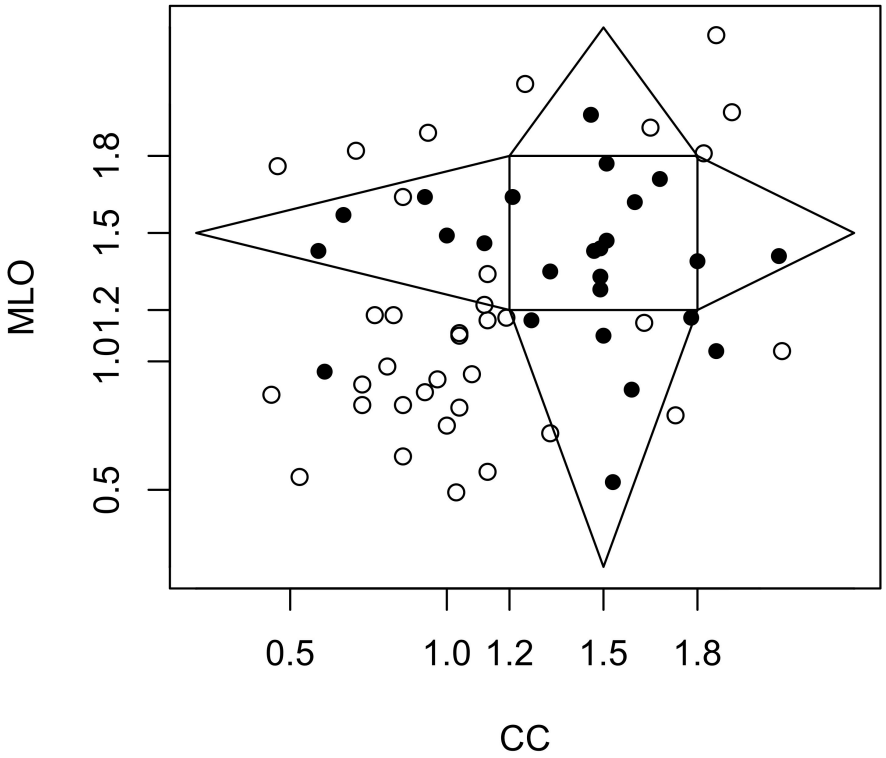
MLO
0.5
1.0
1.2
1.5
1.8
CC

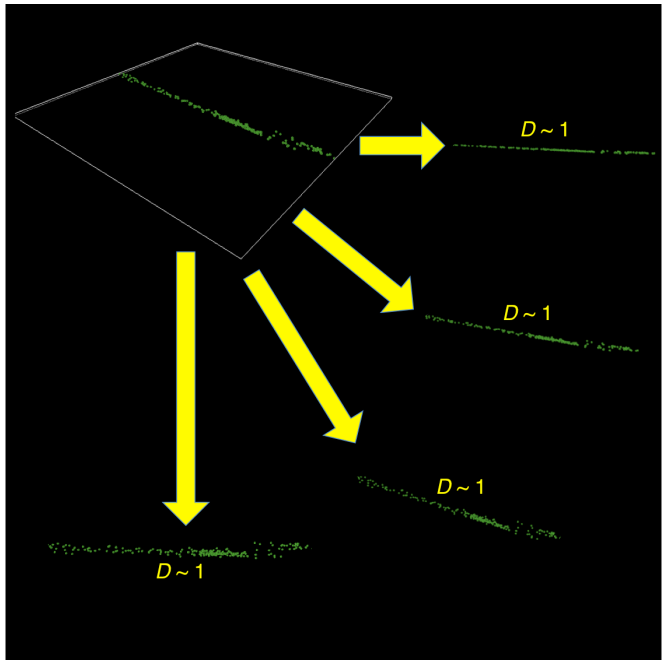
D ~ 1
D ~ 1
D ~ 1
D ~ 1

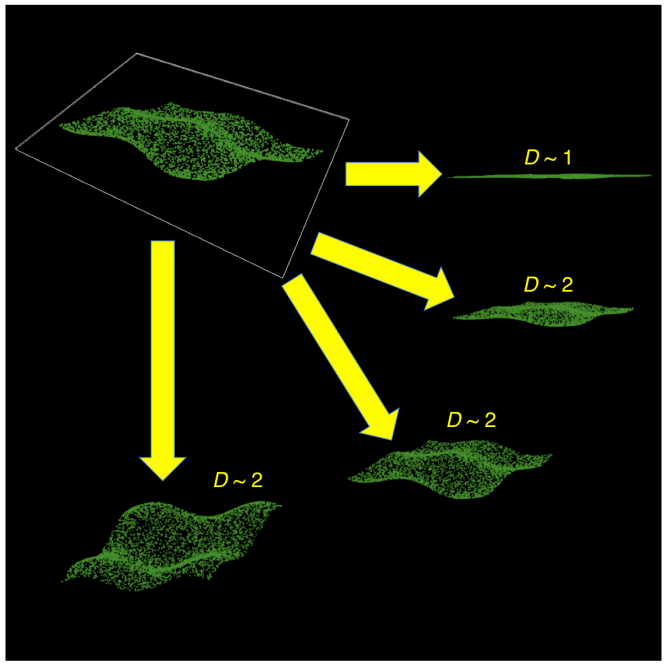
D ~ 1
D ~ 2
D ~ 2
D ~ 2

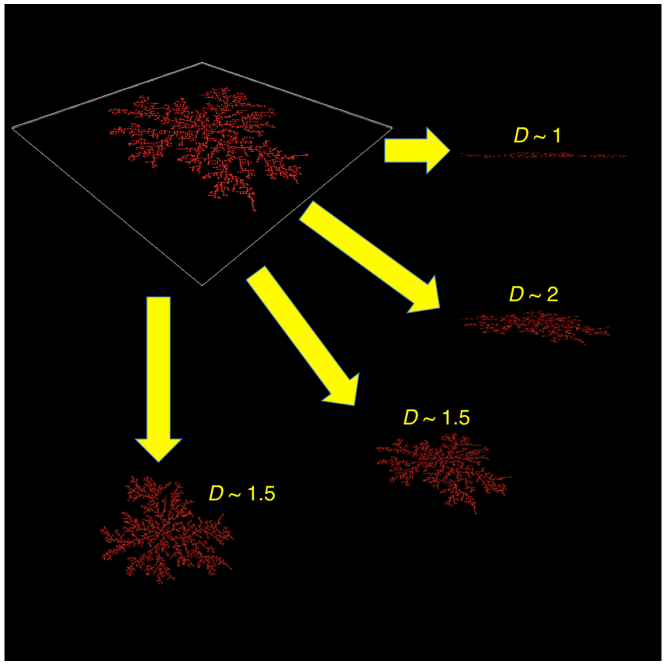
D ~ 1
D ~ 2
D ~ 1.5
D ~ 1.5

Multifractal analysis of skin temperature dynamics of women breasts with and without tumor

E. Gerasimova et al., EPL 104 (2013) 68011
E. Gerasimova et al., Frontiers in Physiology 5 (2014) 176

Evgeniya Gerasimova
Oleg Naimark
Institute of Continuous Media Mechanics UB RAS, Perm, Russia

Olga Gileva
Perm State Academy of Medecine, Perm, Russia

Françoise Argoul
Alain Arneodo
Benjamin Audit
Stéphane G. Roux
Ecole Normale Supérieure de Lyon, France

André Khalil
ComputMaine Laboratory, University of Maine, Orono, USA

Patient investigation

Infrared camera

Breast thermogram

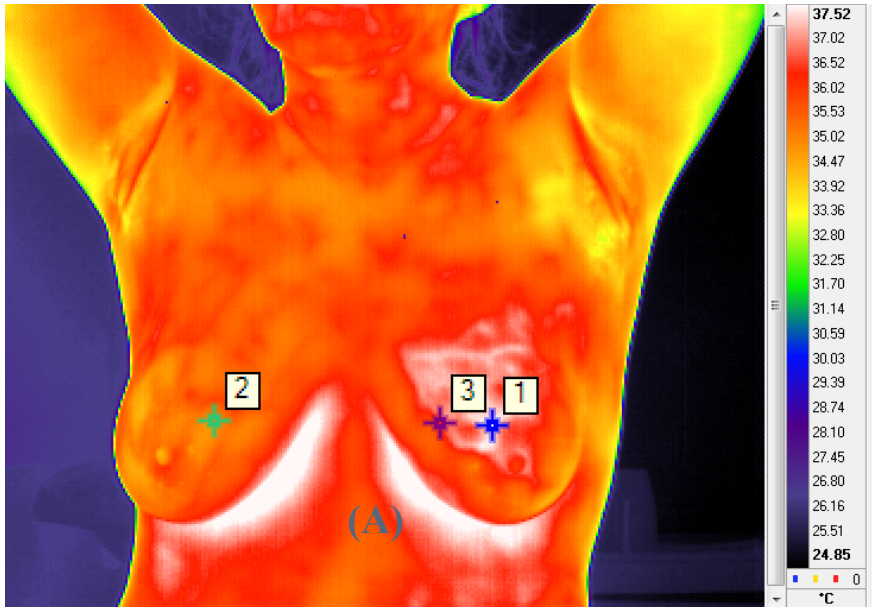

Temperature time series

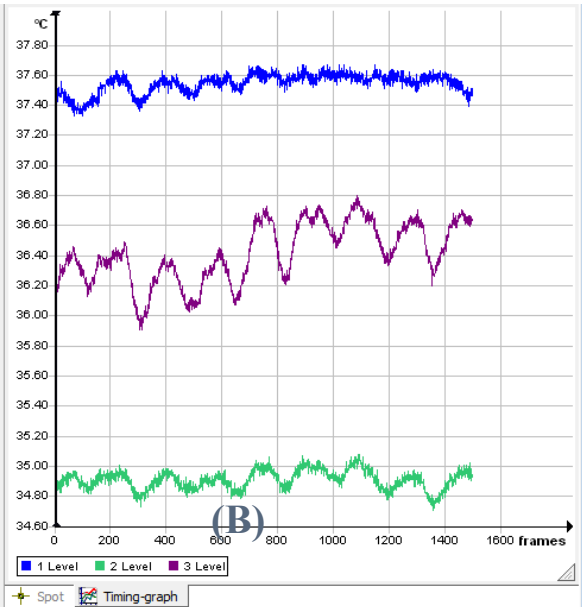

Infrared thermography in oncology

Thermal features are divided into signs and criteria based upon the statistical association with established breast disease.

Thermology signs are:

- Asymmetric and hyperthermic vascular patterns;
- Focal patterns of +2.5° C differential;
- Asymmetric and atypical complexity of a vascular pattern;
- Asymmetric and diffusely hyperthermic (+2° C differential) patterns involving the peri-areolar area or entire breast;
- Localized heat along an abnormal physical contour (edge sign);
- Lack of an adaptive response to an autonomic challenge procedure.

Thermology criteria are:

- Anarchic or complex vascular features;
- Hyperthermic focal patterns greater than 3° C differential;
- Asymmetric and abnormal complexity of a vascular pattern;
- Asymmetric and abnormal physical contour of more than one quadrant of a breast;
- Any combination of the thermology signs.

Power spectrum analysis

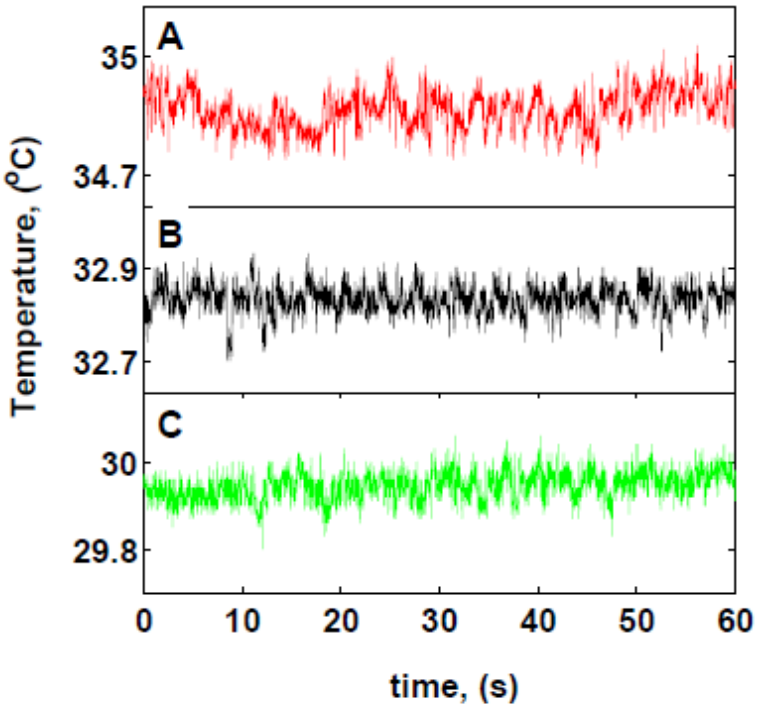

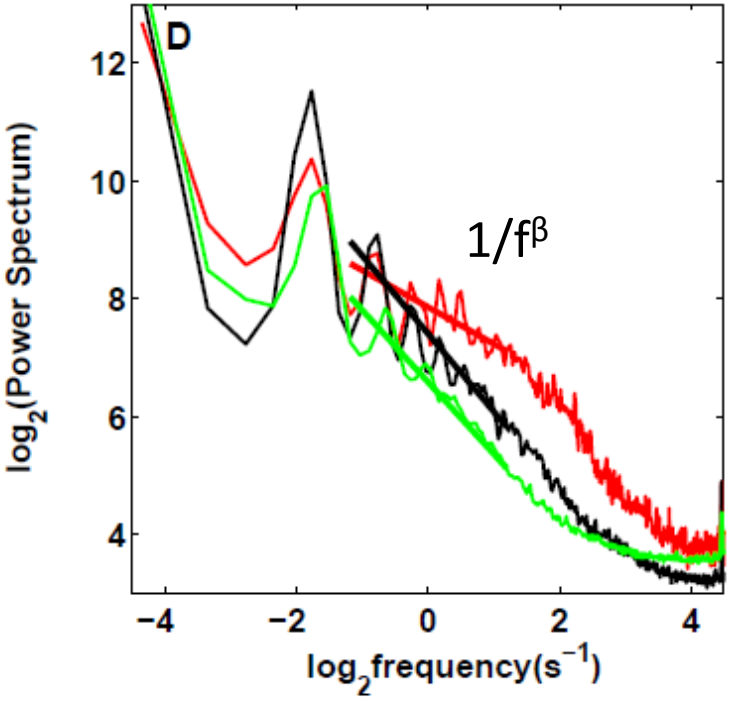

Cancer β=0.62

Opposite β=1.32

Healthy β=1.22

Multifractal analysis of cumulative IR temperature time series

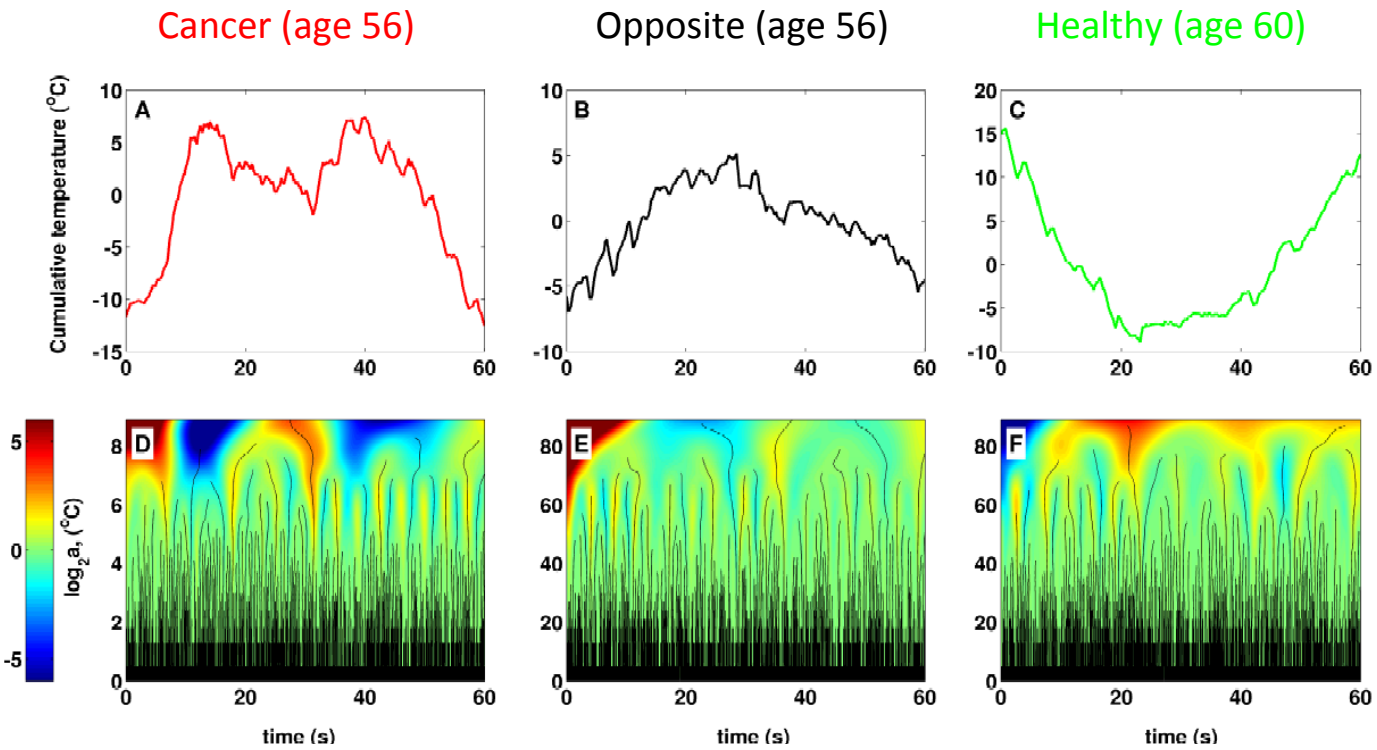

$$W_\psi(x_0,a)=\frac{1}{a}\int_{-\infty}^{+\infty}\Sigma(x)\,\psi\left(\frac{x-x_0}{a}\right)dx$$

$$-1<h_f<0$$

$$0<h_\Sigma=h_f+1<1$$

Compactly supported analyzing wavelets

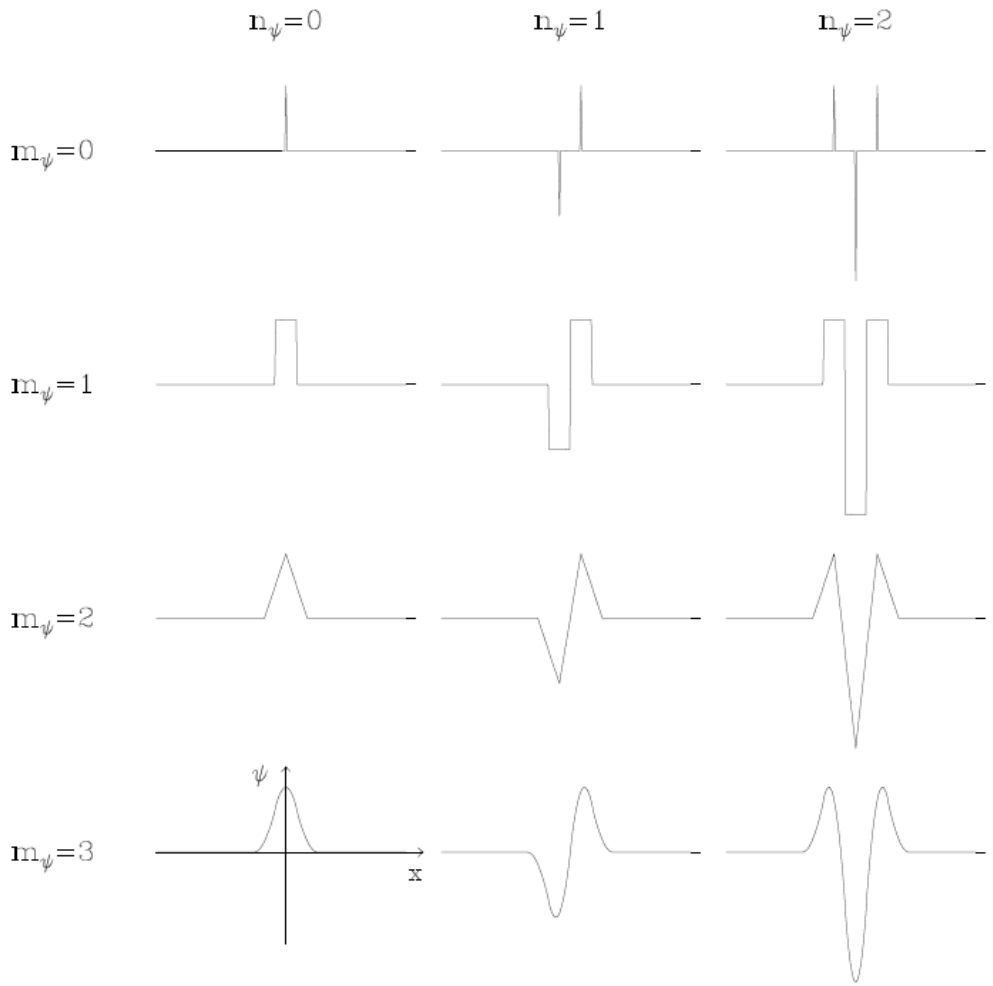

Multifractal analysis of cumulative IR temperature time series

Average over 8x8 pixel^2

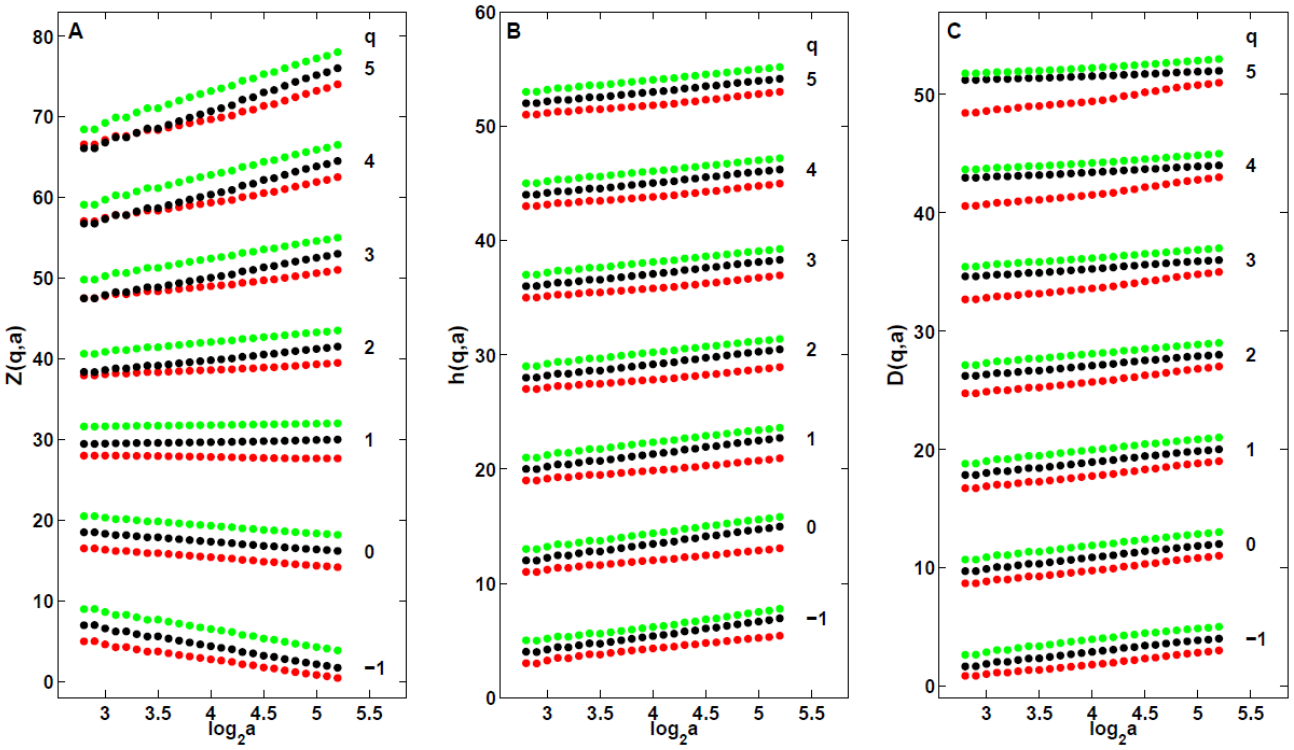

Cancer Opposite Healthy

$$Z(q,a) = \sum_{l \in L(a)} \left[\sup_{\substack{(x,a') \in l \\ a' \le a}} \left| W_\psi(x,a') \right| \right]^q \sim a^{\tau(q)} \qquad (2)$$

$$h(q,a) = \sum_{l \in L(a)} \ln \left| W_\psi(x,a) \right| \hat{W}_\psi(q,L,a)$$

$$\sim h(q) \ln a \qquad (3)$$

$$D(q,a) = \sum_{l \in L(a)} \hat{W}_\psi(q,L,a) \ln \left| \hat{W}_\psi(q,L,a) \right|$$

$$\sim D(q) \ln a \qquad (4)$$

Multifractal spectra of cumulative IR temperature time series

Average over 8x8 pixel^2

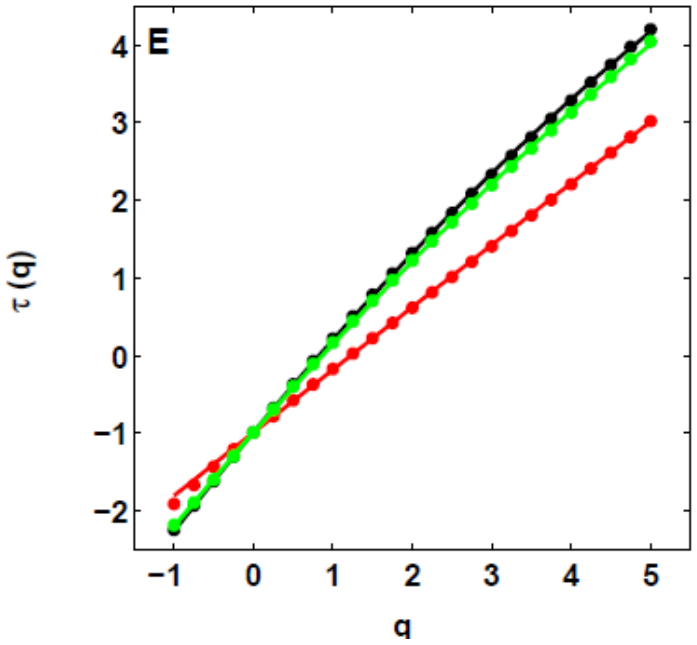

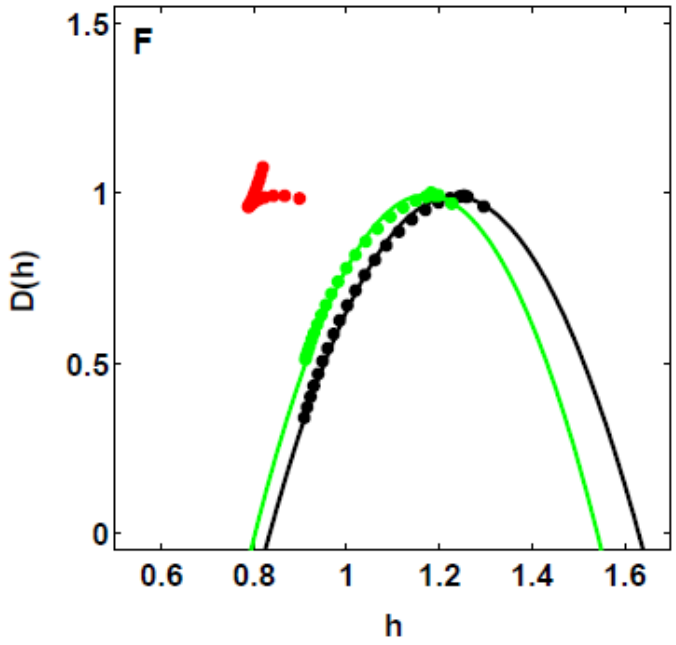

$$\tau(q) = -c_0 + c_1 q - c_2 q^2 / 2$$
$$D(h) = c_0 - (h - c_1)^2 / 2c_2$$

Cancer	[c0, c1, c2]=[0.99, 0.81, 0.0044]
Opposite	[c0, c1, c2]=[0.99, 1.23, 0.080]
Healthy	[c0, c1, c2]=[0.99, 1.171, 0.069]

Evolution of the temperature WT coefficient pdfs across time-scales

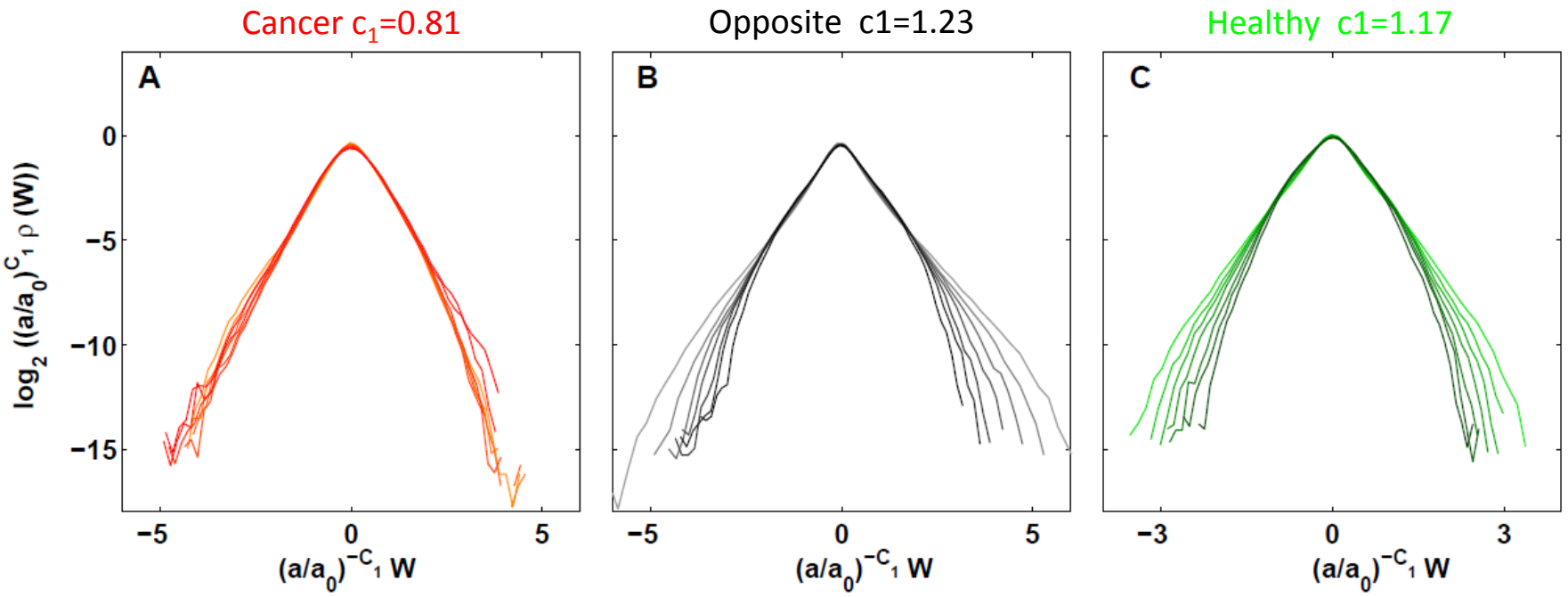

a_0=0.43 s

$$a^H \rho_a(a^H W) = \rho(W)$$

Breast-wide multifractal analysis of skin temperature temporal fluctuations

Patient 20 - Age 56

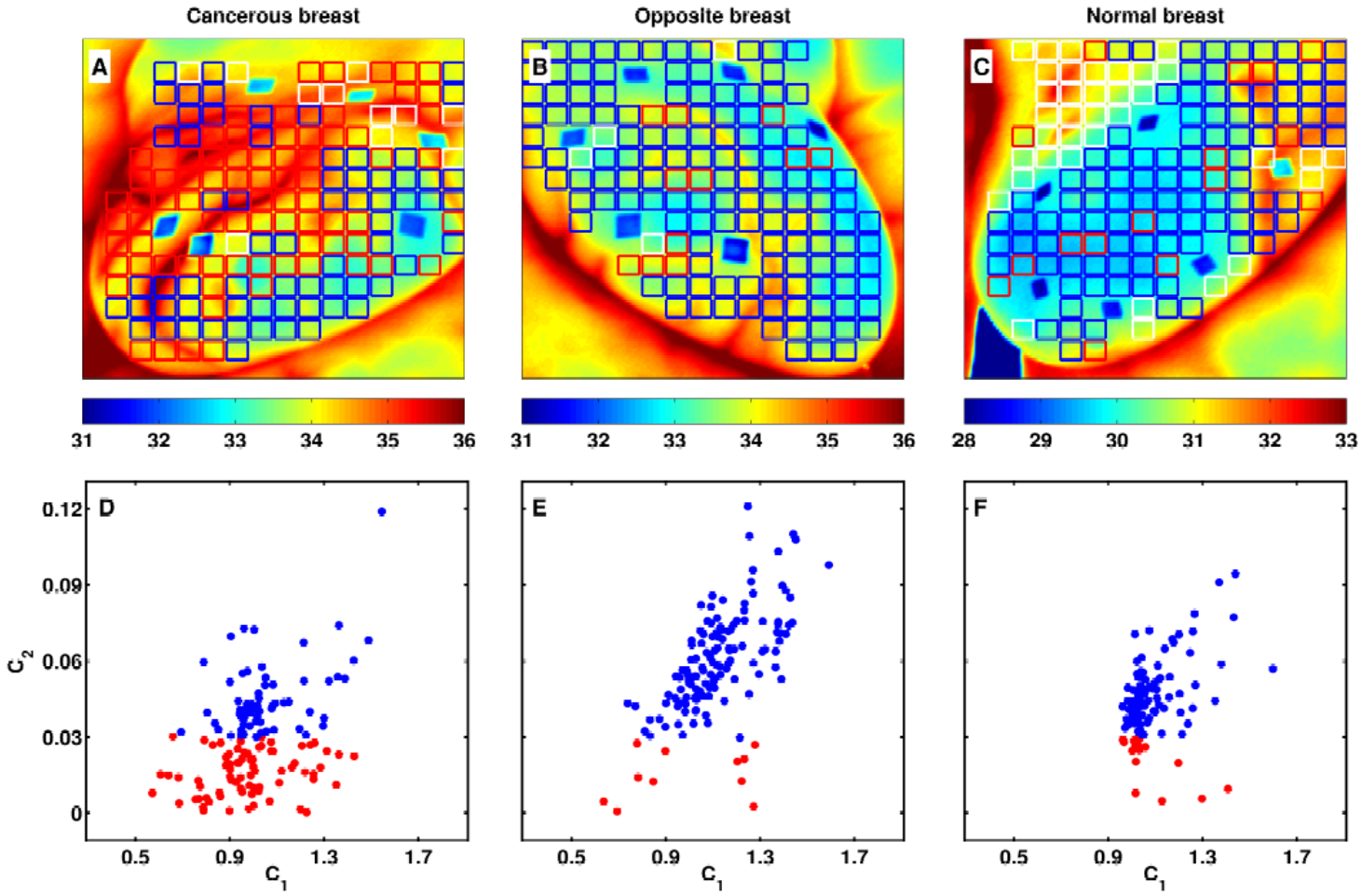

Comparative analysis of both breasts of 33 patients with breast cancer and 14 healthy volunteers

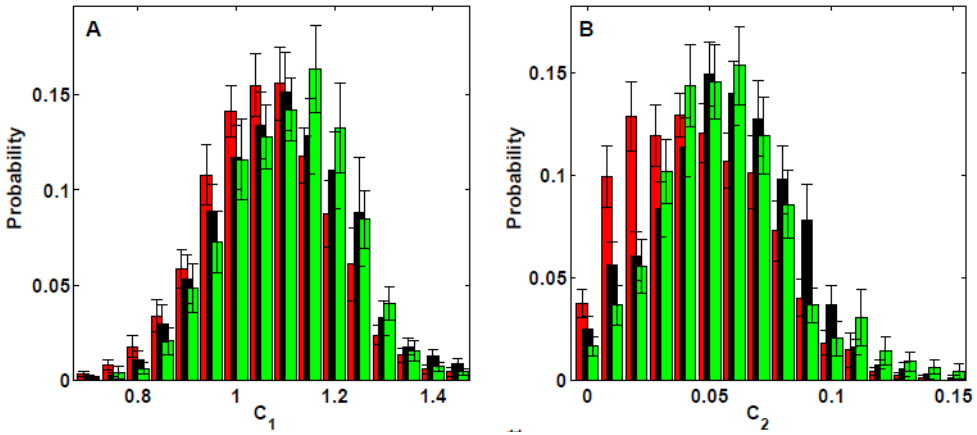

Cancer N=4032 squares
Opposite N=3606 squares
Healthy N=3185 squares

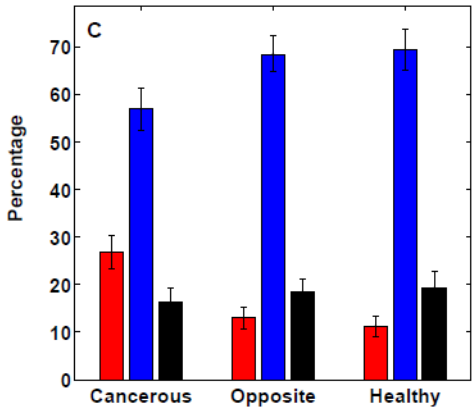

Monofractal $C_2<0.03$
Multifractal $C_2>0.03$
No scaling

Comparison of cancer and opposite breasts

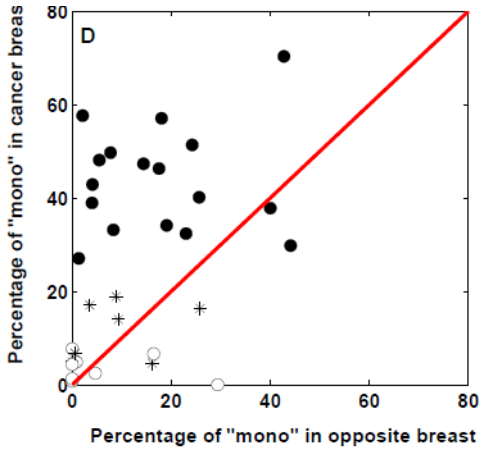

Power spectrum analysis

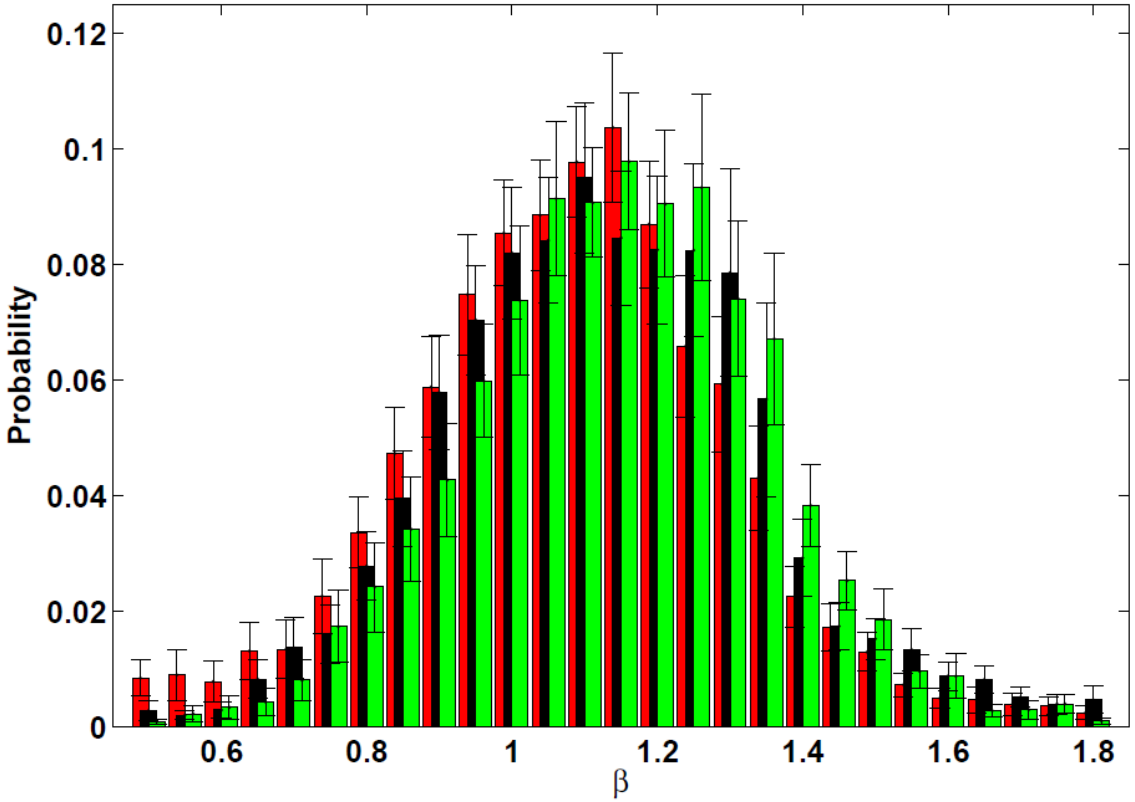

Cancer <β>=1.09±0.01

Opposite <β>=1.14±0.01

Healthy <β>=1.14±0.01

Breast-wide multifractal analysis of skin (cumulative) temperature temporal fluctuations

Patient 33 - Age 37

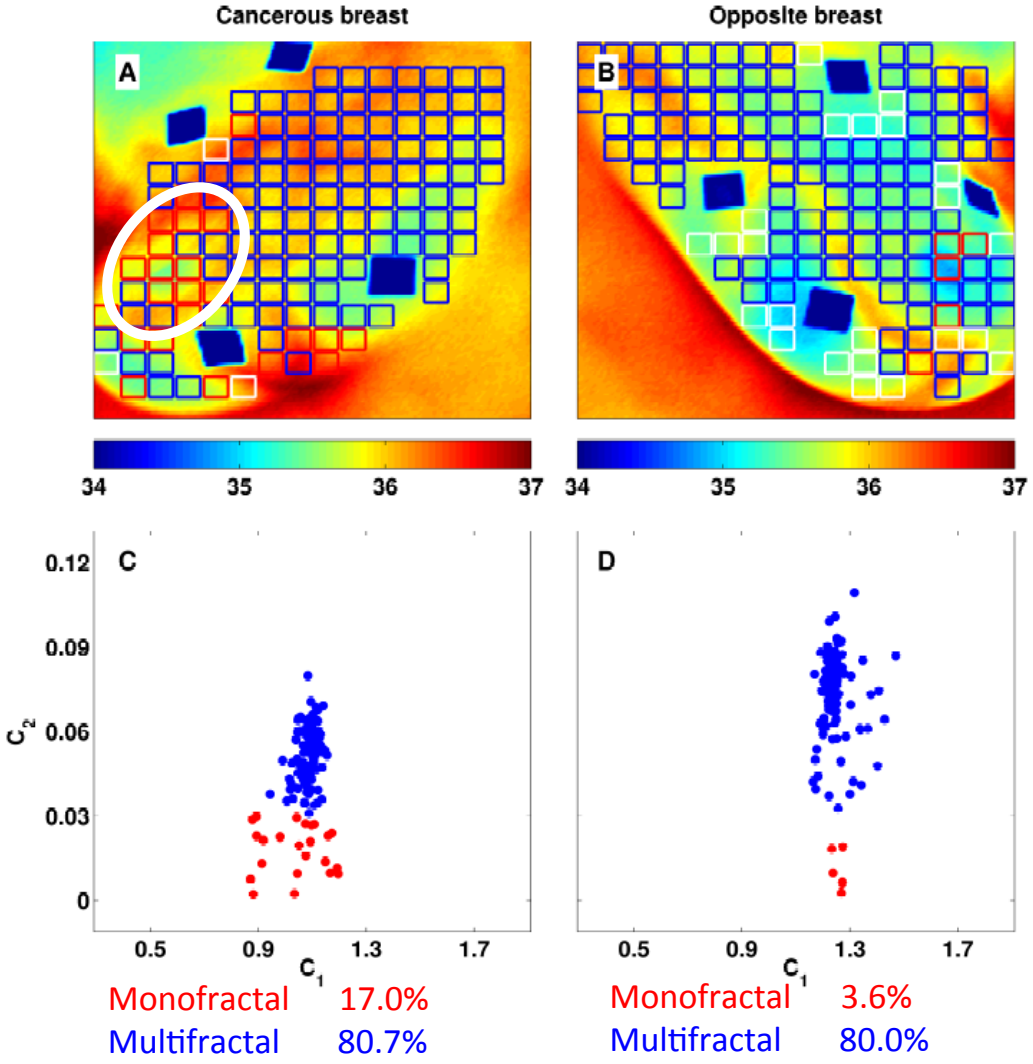

Monofractal 17.0%
Multifractal 80.7%

Monofractal 3.6%
Multifractal 80.0%

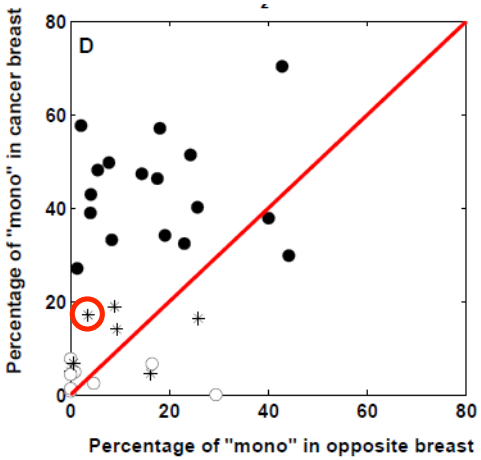

- 18(/32) %mono >27%

+ 7(/33) %mono <27%
but located in the tumor region

o 7(/33) false negatives among
which 4 correspond to deep tumors

CORRECT POSITIONING

Breast-wide multifractal analysis of skin (cumulative) temperature temporal fluctuations

Patient 12 - Age 59

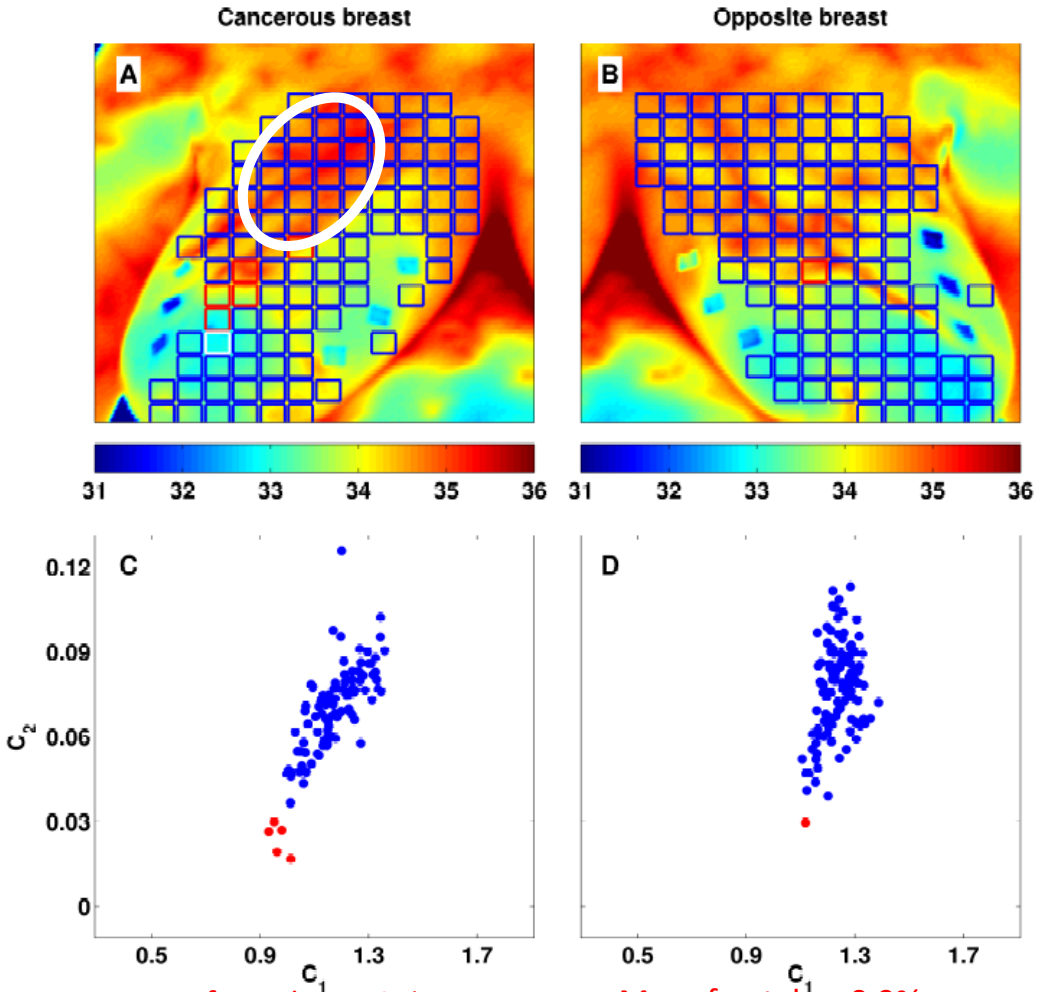

Monofractal 4.9%
Multifractal 94.2%

Monofractal 0.9%
Multifractal 99.1%

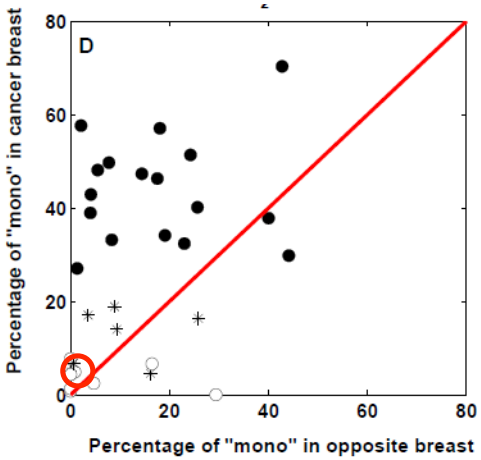

- 18(/32) %mono >27%

+ 7(/33) %mono <27%
but located in the tumor region

o 7(/33) false negatives among
which 4 correspond to deep tumors

FALSE NEGATIVE

Tumor size 1.8 cm depth 12 cm

Breast-wide multifractal analysis of skin (cumulative) temperature temporal fluctuations

Patient 27 – Age 62

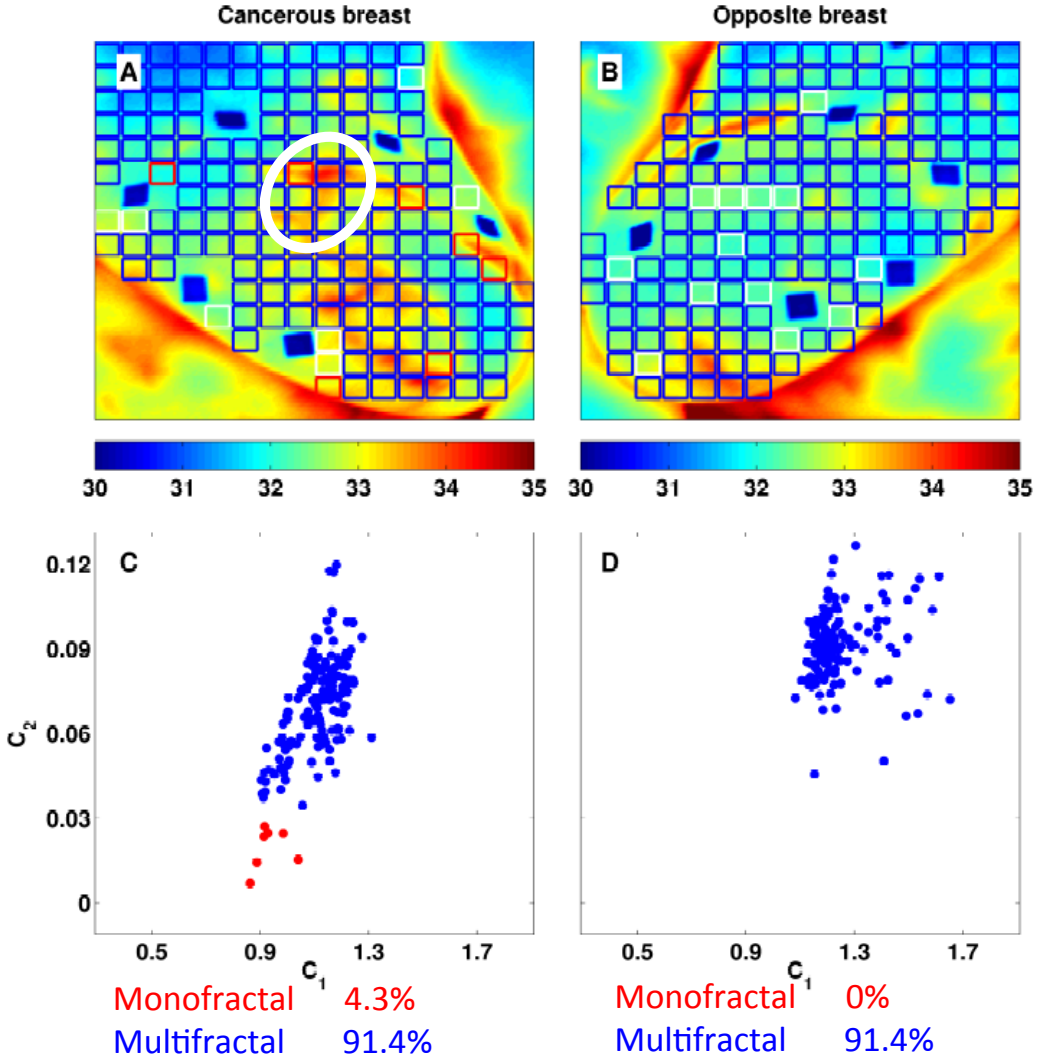

Monofractal 4.3%
Multifractal 91.4%

Monofractal 0%
Multifractal 91.4%

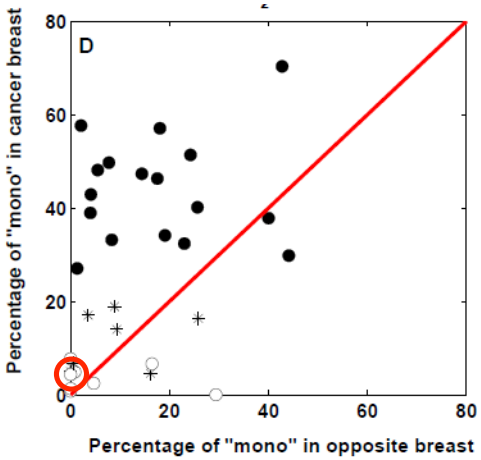

- 18(/32) %mono >27%

+ 7(/33) %mono <27%
but located in the tumor region

o 7(/33) false negatives among
which 4 correspond to deep tumors

FALSE NEGATIVE

Tumor size 2 cm depth 2 cm

Breast-wide multifractal analysis of skin (cumulative) temperature temporal fluctuations

Patient 30 – Age 54

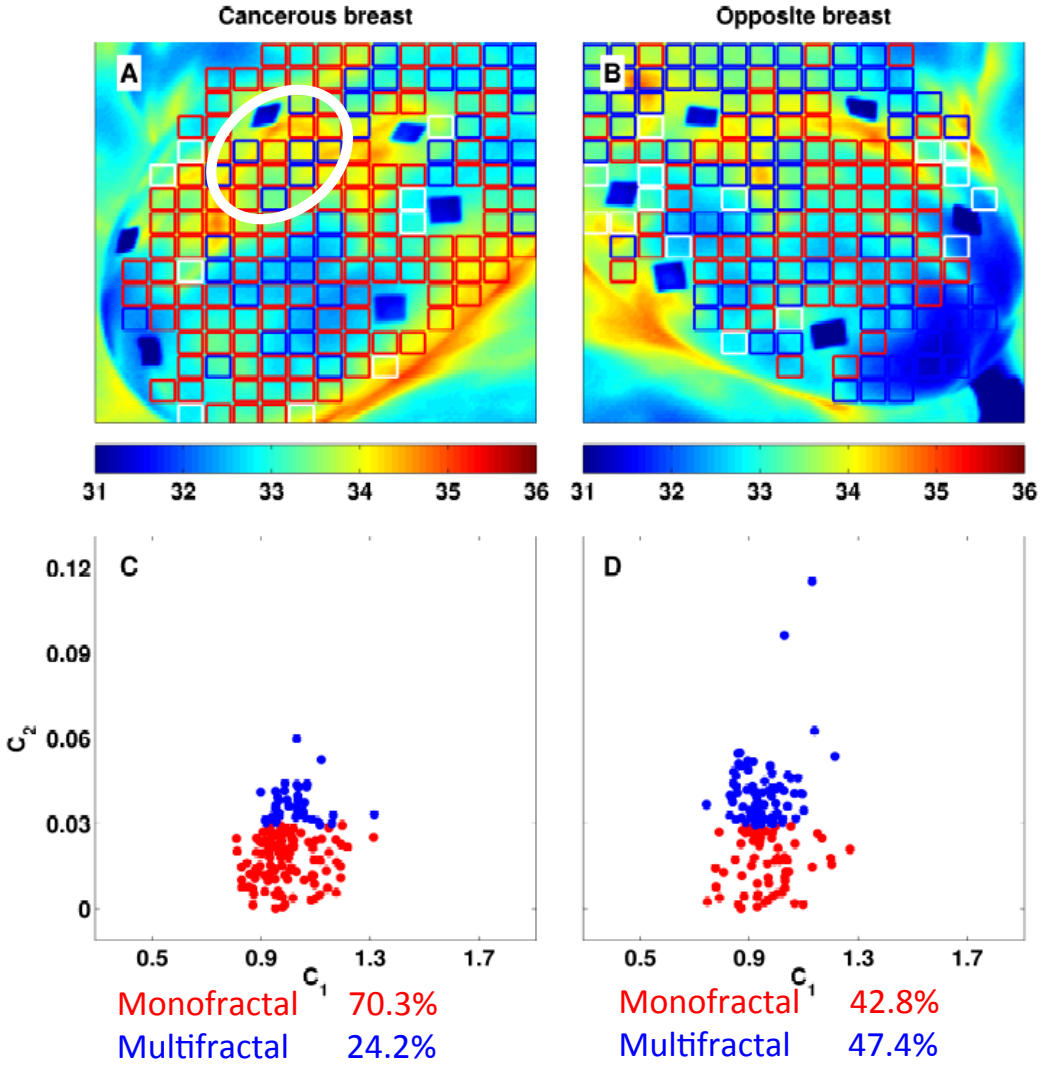

Monofractal 70.3%
Multifractal 24.2%

Monofractal 42.8%
Multifractal 47.4%

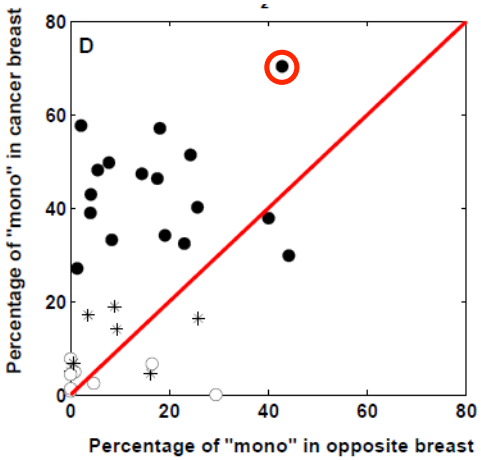

- 18(/32) %mono >27%

+ 7(/33) %mono <27%
but located in the tumor region

o 7(/33) false negatives among
which 4 correspond to deep tumors

5(/32) have sign of physiological changes in opposite breast !!

Comparative analysis of the two breasts of 14 healthy volunteers

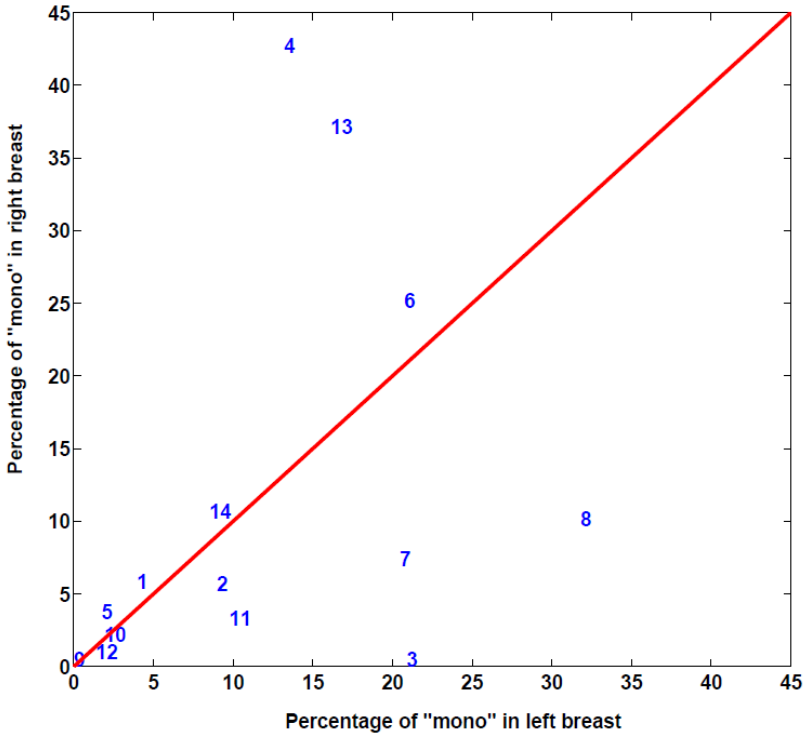

Among the 28 breasts, 4 have an anomalously large (>27%) proportion of monofractal squares

SUMMARY

25(/33) TRUE POSITIVES

4(/28) FALSE POSITIVES

Sensitivity: 76% Specificity: 86%

Breast-wide multifractal analysis of skin (cumulative) temperature temporal fluctuations

Healthy volunteer 5 – Age 26

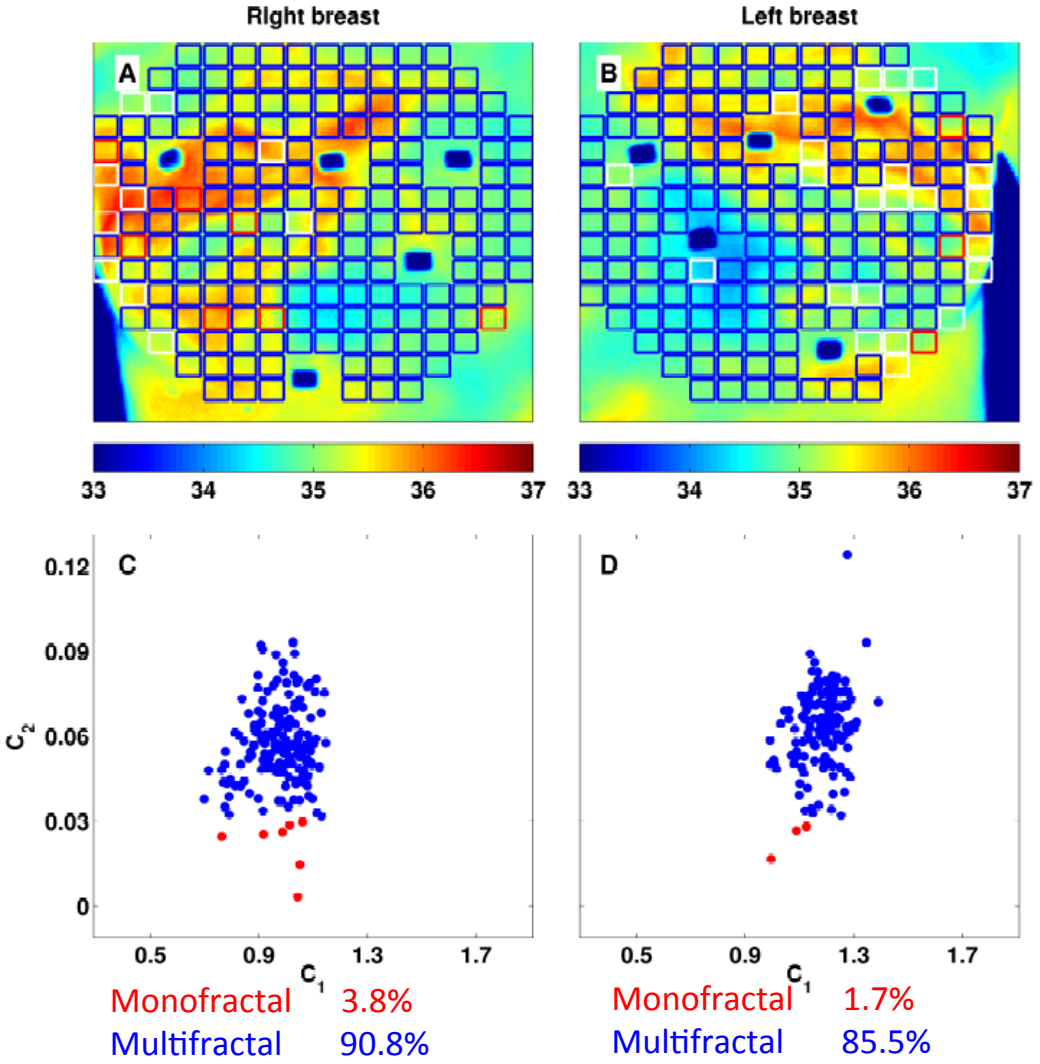

Monofractal 3.8%
Multifractal 90.8%

Monofractal 1.7%
Multifractal 85.5%

Breast-wide multifractal analysis of skin (cumulative) temperature temporal fluctuations

Healthy volunteer 10 – Age 55

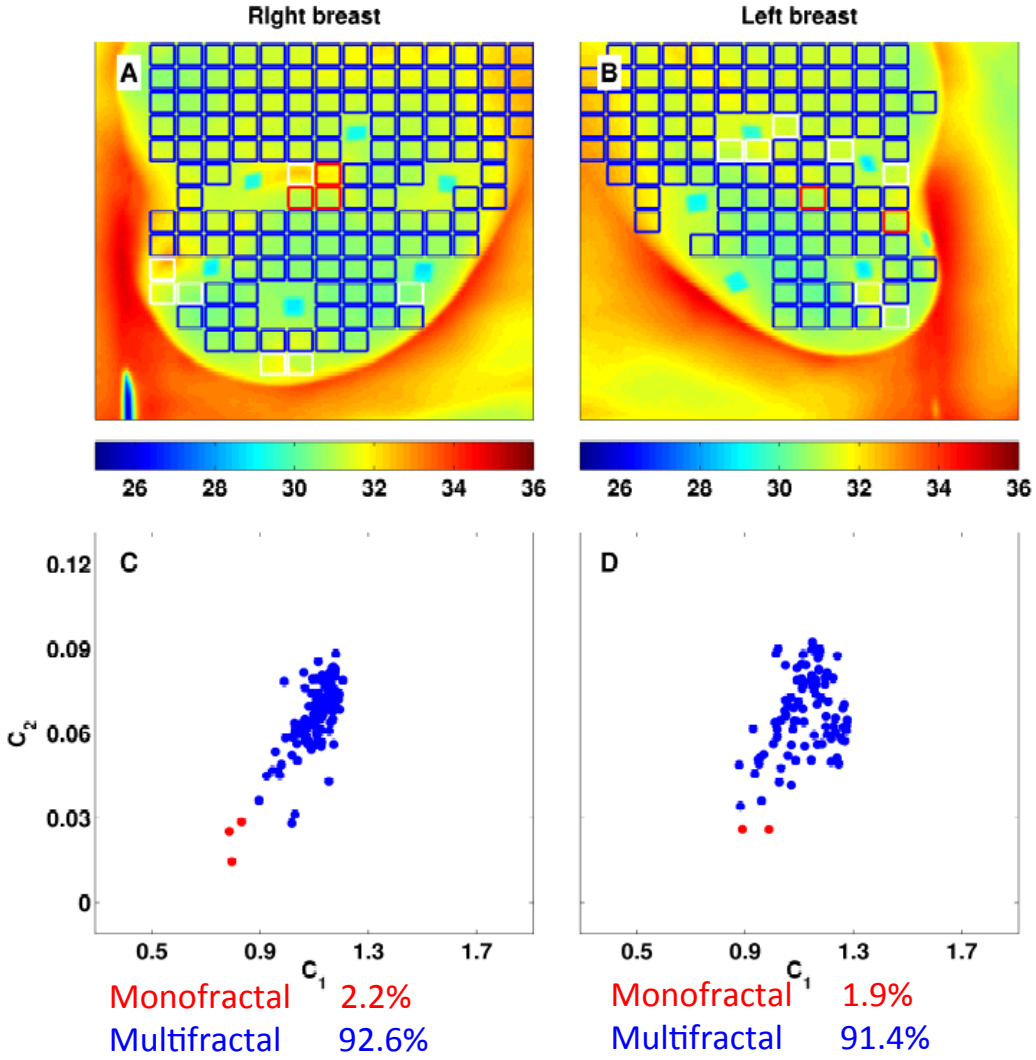

REVIEW

FOCUS ON CANCER

nature medicine

Why don’t we get more cancer? A proposed role of the microenvironment in restraining cancer progression

Mina J Bissell & William C Hines

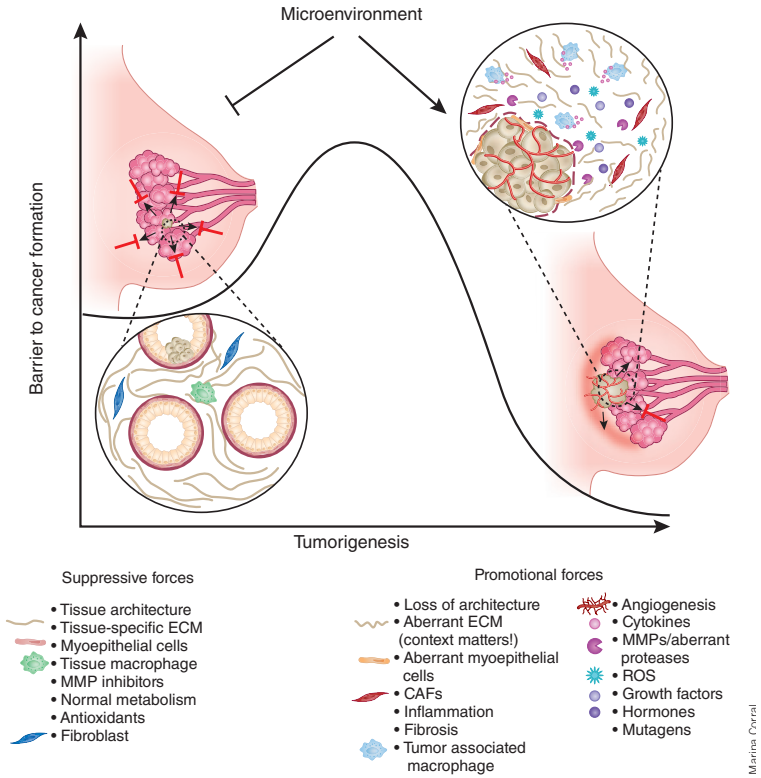

Figure 1 The normal tissue microenvironment acts as a barrier to tumorigenesis. Under conditions of normal tissue homeostasis, the microenvironment exerts suppressive forces to keep occult tumors in check (bottom left in graph). But the microenvironment can also be permissive to tumor growth, and the combination of mutagens, inflammation, growth factors and other tissue-associated promotional forces can breach the barrier to tumor formation, resulting in full-blown cancer (top right).

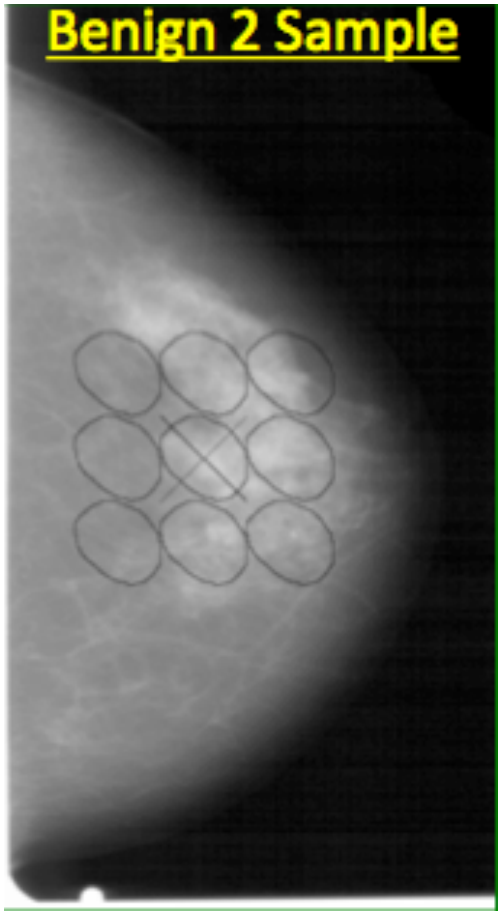

FAT
(H<0.45)

0.45<H<0.55

DENSE
(H>0.55)

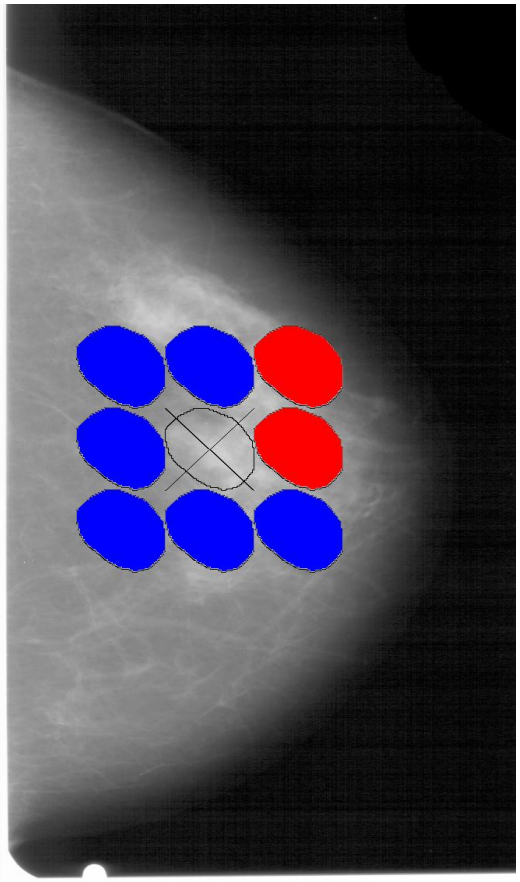

Cancer Sample

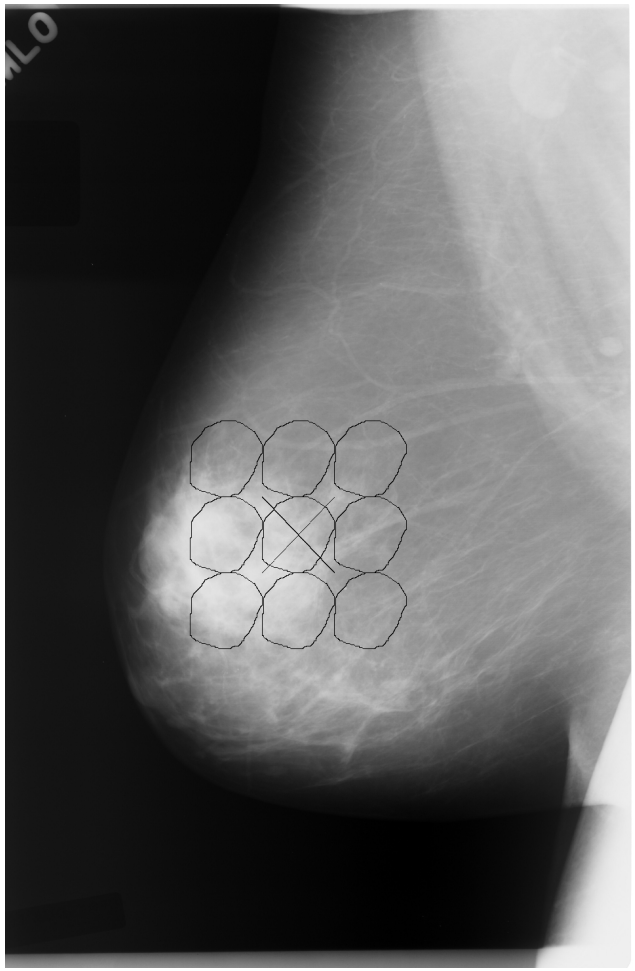

FAT
(H<0.45)

0.45<H<0.55

DENSE
(H>0.55)

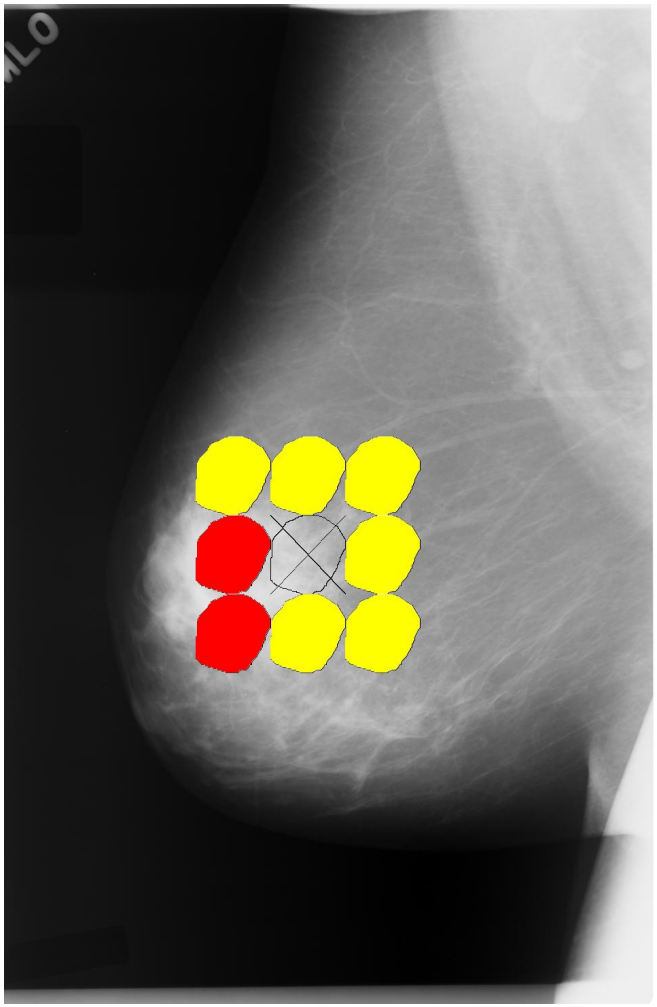

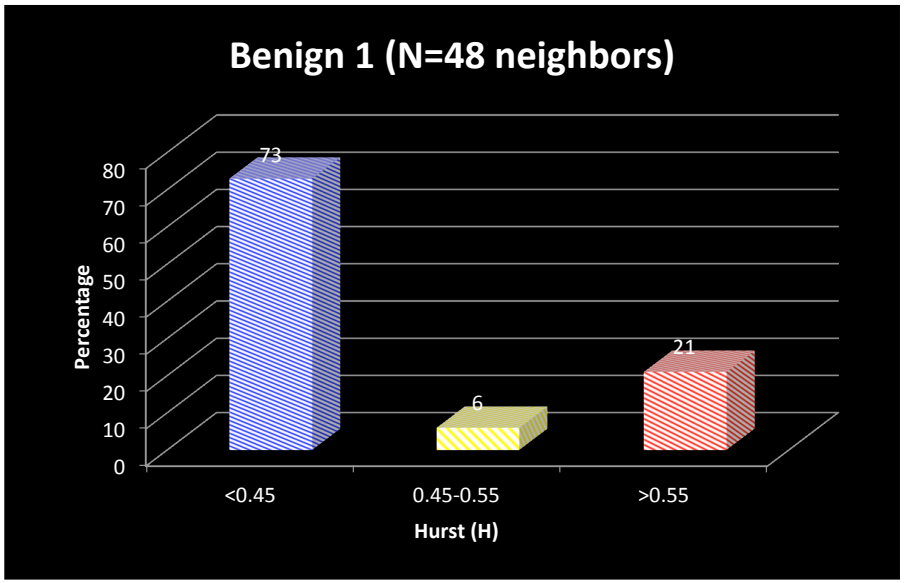
Benign 1 (N=48 neighbors)
Percentage
80
70
60
50
40
30
20
10
0
73
6
21
<0.45
0.45-0.55
>0.55
Hurst (H)

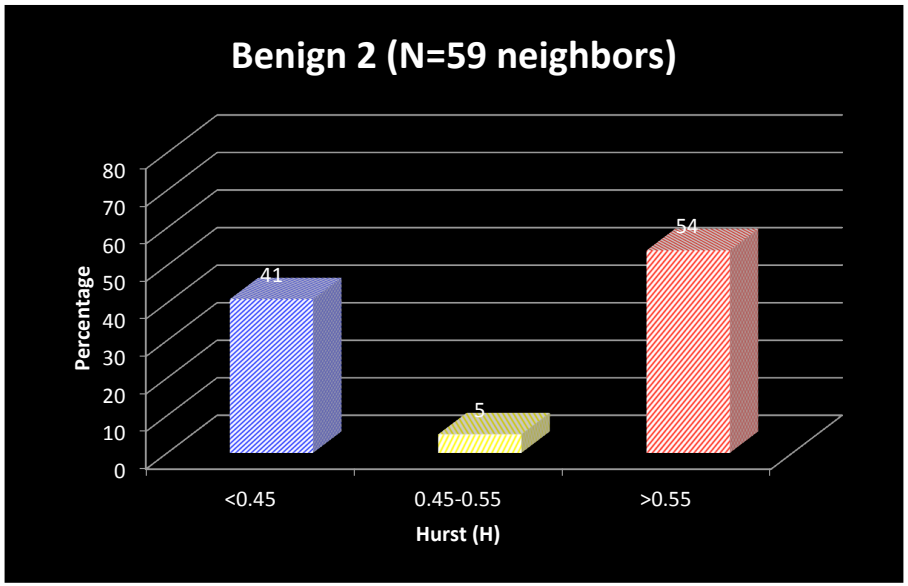
Benign 2 (N=59 neighbors)
Percentage
80
70
60
50
40
30
20
10
0
41
5
54
<0.45
0.45-0.55
>0.55
Hurst (H)

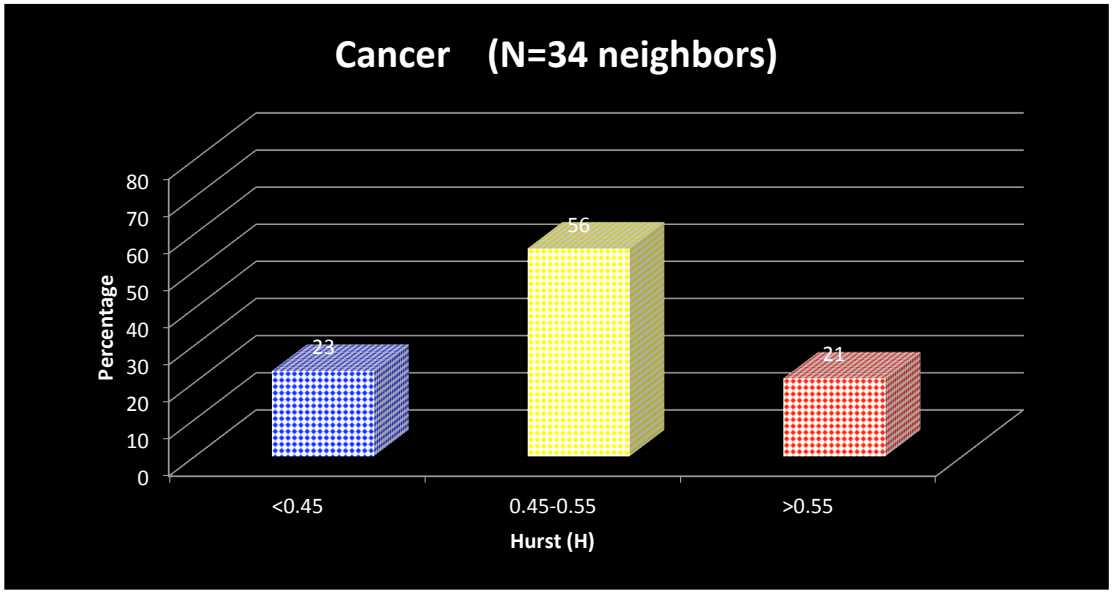
Cancer (N=34 neighbors)
Percentage
80
70
60
50
40
30
20
10
0
23
56
21
<0.45
0.45-0.55
>0.55
Hurst (H)